J. Fluid Mech. (1990), *vol.* 211, *pp.* 123–156
Printed in Great Britain

Breakup of concentric double emulsion droplets in linear flows

By H. A. STONE[1] AND L. G. LEAL[2]

[1] Division of Applied Sciences, Harvard University, Cambridge, MA 02138, USA

[2] Department of Chemical Engineering, California Institute of Technology, Pasadena, CA 91125, USA

(Received 11 April 1989)

The behaviour of concentric double emulsion droplets in linear flows is examined analytically, for the case when both fluid–fluid interfaces remain nearly spherical, and numerically, for the effect of finite interface deformation. The theoretical analysis is used to calculate the velocity fields interior and exterior to the particle, the first effects of flow-induced deformation, and the effective viscosity of a dilute emulsion of compound droplets. The numerical simulations allow for a complete investigation of the finite deformation of both the outer drop and the encapsulated particle. For concentric multiphase particles, there appear to be two distinct mechanisms of globule breakup: (i) continuous extension of the globule corresponding to non-existence of a steady particle shape or (ii) contact of the two interfaces at the globule centre, owing to incompatibility of the steady inner and outer interface shapes, even though the globule is only modestly deformed. Finally, the effect of different flow-types, i.e. uniaxial or biaxial extensional flows, is shown, in one example, to suggest breakup of the inner droplet even though the outer droplet maintains a steady shape.

1. Introduction

Fundamental studies of the dynamics of encapsulated particles or drops have appeared recently in the fluid mechanics literature, cf. the review article by Johnson & Sadhal (1985). An encapsulated particle is a particle or drop (or, more generally, multiple particles or drops) that is completely engulfed by a second immiscible fluid drop. This larger drop is itself suspended in an immiscible fluid. In order to distinguish these compound 'double emulsion' drops from single-phase drops, which have been studied widely for many years, we will follow the precedent of previous authors and call them globules.

Globules exist in a wide variety of technologically significant processes. The most well-known application of double emulsions is their use as liquid membranes for selective mass transport. The use of liquid membranes for the separation of hydrocarbons was proposed originally by Li (1971*a*, *b*) and has subsequently been extended to artificial blood oxygenation, water purification, recovery of heavy metals, and even the controlled release of drugs (Maugh 1976). The globules are efficient for mass transfer processes because of the high interfacial area per unit volume that can be generated, coupled with the short diffusion distances associated with transport between phases. The globules typical of these applications are very small (the undeformed radii are generally 10^{-3}–10^{-1} cm) so that inertial effects are small and Stokes equations can be used as a first approximation. Because aspects of

several industrial operations involve multiphase droplets rising through an otherwise quiescent fluid, the majority of existing theoretical analyses of these systems have focused on the sedimentation problem.

Initial low-Reynolds-number studies of streaming flow past drops coated with thin fluid films were presented by Johnson (1981) and Johnson & Sadhal (1983). Rushton & Davies (1983) studied the translation of concentric spherical droplets in an infinite fluid. This work has been extended recently by Sadhal & Oguz (1985) who allowed for non-concentric, though spherical, drops and accounted for the relative motion of the inner and outer drops, leading to an investigation of the stability of eccentric configurations of encapsulated particles. Finally, the first effects of inertia for concentric spherical drops were calculated by Brunn & Roden (1985). These analyses all have in common the assumption that the shapes and locations of the fluid–fluid interfaces are known a priori.

The first corrections to the inner and outer drop shapes were obtained by Chervenivanova & Zapryanov (1988), based upon the velocity fields of Sadhal & Oguz. The most interesting result of the analysis is that both drops deform at zero Reynolds numbers, unlike a single sedimenting drop which remains exactly spherical at zero Reynolds number, independent of the magnitude of the capillary number (Taylor & Acrivos 1964). Further, the flow created by a sedimenting globule causes the outer drop to deform into a prolate spheroid while the inner drop deforms into an oblate spheroid. Of course, these deformation analyses are limited to asymptotically small distortions from a sphere.

High-Reynolds-number studies of encapsulated particles have been concerned primarily with centring of bubbles in fluid droplets (Tsamopoulos & Brown 1987). These problems arise, for example, in the formation of spherosymmetric shells of metal and glass that are used as fuel targets in inertial confinement fusion studies and in particles that have been suggested as additives in high-strength composite systems. It is interesting to note that the interaction between flow-induced prolate and oblate shapes of the inner and outer droplets, observed in the low-Reynolds-number work discussed above, is also found in these higher-Reynolds-number studies.†

One aspect of the dynamics of compound drop (or globule) motion that has not been studied from a theoretical point of view is the condition (or conditions) for globule breakup. It is evident that the effective use of compound drops as liquid membranes will be hindered by breakup of the globules. The only experimental work that we know of is due to Ulbrecht, Stroeve & Prabodh (1982) and Stroeve & Varanasi (1984), who conducted experimental studies of the breakup of double emulsions in simple shear flows. These studies suggest that useful predictions can be achieved by direct analogies with single-phase drop breakup studies, at least when the globule contains many subdrops, as is often the case in double emulsions. Closely related to this work on compound drops is the work of Davis & Brenner (1981), who used a small deformation analysis to examine the deformation of a fluid drop, with a solid sphere occluded at the centre, in a simple shear flow. Under certain conditions (the viscosity ratio of the two fluid phases is order one and the flows are weak), the presence of the solid phase appears to destabilize the globule in the sense that the globule is more deformed (and thus possibly closer to breakup) than it would be without the occluded solid. Davis & Brenner also calculated the rheological properties of a dilute suspension of these encapsulated particles.

† We wish to thank Professor R. A. Brown for directing our attention to these investigations.

Our concern in the present paper is the deformation and breakup of compound multiphase droplets in a general linear flow at low Reynolds number. The corresponding problem of deformation and breakup of single-phase droplets in the creeping flow limit owing to an imposed velocity gradient has been widely studied and interested readers are referred to review articles by Acrivos (1983) and Rallison (1984). An important inference from these latter studies is the necessity of studying the deformation and breakup problem in so-called strong flows, in which the magnitude of the strain-rate exceeds the magnitude of the vorticity (e.g. Bentley & Leal 1986). Hence, in the present work, we examine the effect of a general linear flow on a concentric double emulsion drop using a small deformation approximation, and the specific case of an axisymmetric extensional flow using numerical methods based upon the boundary integral technique. The *concentric* configuration is simpler than *eccentrically* configured globules and more straightforward than the case of multiple subdrops, but it is not just a mathematical diversion. Double emulsions consisting of a drop containing a single internal drop have been prepared experimentally by Florence & Whitehill (1981). Furthermore, this study will generalize the results of Davis & Brenner (1981) to account for the presence of an occluded drop of arbitrary viscosity and to consider a general linear flow instead of a simple shear flow.

The hydrodynamic stability of the concentric drop configuration has not been examined here. The thermodynamic stability of similar multiphase drops, which depends on the interfacial tensions of all three fluid–fluid pairs, was addressed by Torza & Mason (1969, 1970). Also, Torza & Mason (1970) briefly discussed the behaviour of double emulsions in simple shear flows.

The small-deformation theory presented in the first part of this paper demonstrates the initial effects of flow-induced deformation and examines the effects of the different fluid properties. In addition, the effective viscosity of a dilute emulsion of these particles is calculated. Cases of finite deformation and possible breakup are addressed in the second part of this paper using a complete numerical solution. As suggested by Davis & Brenner, the presence of the inner droplet may lead to globule breakup at a smaller capillary number than would have been necessary had the inner phase not been present. The numerical results illustrate that breakup may occur owing to large-scale stretching of the globule into a cylindrical shape, similar in many respects to the breakup of single-phase droplets. However, the numerical simulations also illustrate systems where globule breakup is more likely to occur because the inner droplet causes the outer interface to rupture without excessive globule deformation. In addition, an example is documented where the *inner* droplet approaches breakup because of flow-induced deformation caused by circulation inside the globule even though the globule itself maintains a steady, nearly spherical shape.

2. Problem statement

Consider the double emulsion droplet shown in figure 1. We restrict our study to the case where the centres of mass of the two droplets remain coincident. The undeformed radius of the outer droplet is R_1, the undeformed radius of the inner droplet is R_2 and $\kappa = R_2/R_1$. The three distinct Newtonian fluid phases are immiscible with viscosities μ_i and densities ρ_i. The interfacial tension (assumed constant) of the ij interface is denoted by σ_{ij}. With respect to a coordinate system fixed to the centre of the globule, we consider the case where the imposed flow field varies linearly with position. This provides a good approximation for many general flows for which the

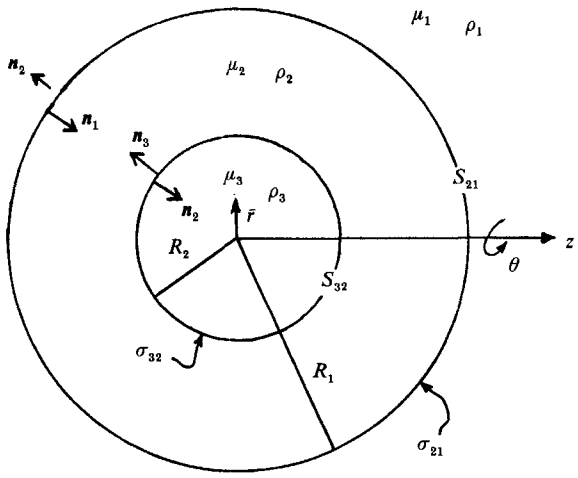

FIGURE 1. Concentric double emulsion droplet. Definition of variables.

velocity gradient varies on a lengthscale that is large compared to R_1. Thus, far from the droplet, we assume that the velocity is given by

$$\boldsymbol{u}_\infty = \boldsymbol{\Gamma}\cdot\boldsymbol{x}, \tag{1}$$

where $\boldsymbol{\Gamma}$ is the velocity gradient tensor, which is traceless as a consequence of continuity. Alternatively, the undisturbed velocity field may be decomposed into a symmetric and an antisymmetric part, in which case (1) may be written as

$$\boldsymbol{u}_\infty = \boldsymbol{E}\cdot\boldsymbol{x} + \tfrac{1}{2}\boldsymbol{\omega}\wedge\boldsymbol{x} \tag{2}$$

where $\boldsymbol{E}$, the rate-of-strain-tensor, is the symmetric part of $\boldsymbol{\Gamma}$ and $\boldsymbol{\omega}$ is the vorticity.

In this paper we present an analytic solution for the velocity and pressure fields internal and external to the globule for the general linear flow (1) or (2). These analytic calculations are restricted to the case where both the inner and outer droplets remain nearly spherical and include the first corrections to the shapes of the droplets. Specific computations are presented for the case of axisymmetric extensional flows where $\omega = \boldsymbol{O}$ and $\boldsymbol{E}$ has the diagonal form

$$\boldsymbol{E} = \pm\tfrac{1}{2}G\begin{pmatrix} -1 & 0 & 0 \\ 0 & -1 & 0 \\ 0 & 0 & 2 \end{pmatrix}. \tag{3}$$

The + sign corresponds to a uniaxial extensional flow and the − sign corresponds to a biaxial extensional flow. The term G denotes the shear rate.

When significant deformation occurs, as must certainly happen if the globule begins to break, the analytic (small-deformation) procedure breaks down and we must resort to a numerical solution of the problem. This is described in §4. In this case, we also restrict our calculations to the axisymmetric flows described by (3).

For the small droplets typical of many processes involving double emulsions, inertial effects are negligible and the fluid motion in each phase is governed by the quasi-steady Stokes equations. Non-dimensionalizing all lengths by $l_c = R_1$, velocities

by $u_c = GR_1$, times by $t_c = G^{-1}$ and the pressure in phase i by $p_{c_i} = \mu_i u_c / R_1$, the governing equations for phase i are

$$\nabla^2 \boldsymbol{u}_i = \nabla p_i, \tag{4a}$$

$$\nabla \cdot \boldsymbol{u}_i = 0. \tag{4b}$$

Here $(\boldsymbol{u}_i, p_i)$ represent the dimensionless velocity and pressure fields in phase i. The boundary conditions for the three phases are

$$\boldsymbol{u}_1 = \boldsymbol{\Gamma} \cdot \boldsymbol{x}, \quad p \to p_\infty \quad \text{as } |\boldsymbol{x}| \to \infty, \tag{5a}$$

$$\boldsymbol{u}_1 = \boldsymbol{u}_2 \quad \text{for } \boldsymbol{x}_s \in S_{21}, \tag{5b}$$

$$\boldsymbol{u}_2 = \boldsymbol{u}_3 \quad \text{for } \boldsymbol{x}_s \in S_{32}, \tag{5c}$$

$$\boldsymbol{n}_2 \cdot \boldsymbol{T}_1 - \lambda_{21} \boldsymbol{n}_2 \cdot \boldsymbol{T}_2 = \frac{1}{\mathbb{C}_o} \boldsymbol{n}_2 (\nabla_s \cdot \boldsymbol{n}_2) \quad \text{for } \boldsymbol{x}_s \in S_{21}, \tag{5d}$$

$$\boldsymbol{n}_3 \cdot \boldsymbol{T}_2 - \lambda_{32} \boldsymbol{n}_3 \cdot \boldsymbol{T}_3 = \frac{\Omega}{\mathbb{C}_o \lambda_{21}} \boldsymbol{n}_3 (\nabla_s \cdot \boldsymbol{n}_3) \quad \text{for } \boldsymbol{x}_s \in S_{32}, \tag{5e}$$

where

$$\lambda_{21} = \frac{\mu_2}{\mu_1}, \quad \lambda_{32} = \frac{\mu_3}{\mu_2}, \quad \Omega = \frac{\sigma_{32}}{\sigma_{21}},$$

$$\mathbb{C}_o = \frac{GR_1 \mu_1}{\sigma_{21}} \quad \text{and we also define } \mathbb{C}_i = \frac{GR_2 \mu_2}{\sigma_{32}} = \frac{\mathbb{C}_o \lambda_{21} \kappa}{\Omega}.$$

The stress tensor $\boldsymbol{T}$ has the usual definition

$$\boldsymbol{T} = -p\boldsymbol{I} + \nabla \boldsymbol{u} + (\nabla \boldsymbol{u})^{\mathrm{T}}.$$

In these equations S_{ij} denotes the interface separating phases i and j, $\boldsymbol{n}_i$ is the unit normal directed outward from phase i and $\nabla_s \cdot \boldsymbol{n}$ is the local mean curvature of the interface (see figure 1). The *outer* capillary number $\mathbb{C}_o$ is defined using the properties of phase 1 and provides a measure of viscous forces responsible for deformation of the globule relative to interfacial tension forces that resist deformation. Likewise, $\mathbb{C}_i$ denotes a representative capillary number for the inner drop. The dimensionless parameters $\lambda_{21}, \lambda_{32}$ and Ω represent ratios of fluid viscosities and interfacial tensions, respectively.

The fluid–fluid interfaces evolve according to the kinematic conditions, which may be stated as

$$\frac{\mathrm{d}\boldsymbol{x}_s}{\mathrm{d}t} = \boldsymbol{n}_i (\boldsymbol{u}_i \cdot \boldsymbol{n}_i), \tag{6}$$

where $\boldsymbol{x}_s$ denotes a point on the interface.

We are interested in studying the deformation and breakup of double emulsion droplets as a function of the five dimensionless parameters: $\lambda_{21}, \lambda_{32}, \mathbb{C}_o, \mathbb{C}_i$ (or Ω) and $\kappa = R_2/R_1$. Furthermore, in addition to direct dependence on $\mathbb{C}_o$, the type of external flow, for example biaxial or uniaxial extensional flow, will play a role in the breakup problem and will be studied numerically.

The study of time-dependent phenomena using the quasi-steady Stokes equations requires that both local and convective inertial effects be small compared to viscous effects. For steady flow situations this requires that

$$\frac{\rho G R_1^2}{\mu} \ll 1, \quad \frac{\rho \sigma R_1}{\mu^2} \ll 1.$$

The degree of interface deformation is characterized by the dimensionless deformation parameter $D = (L-B)/(L+B)$, where L and B represent the half-length and half-breadth of the interface position, respectively. The half-length L will always be measured in the z-direction and the half-breadth B in the radial ($\bar{r}$) direction (see figure 1). With this definition, prolate spheroidal shapes are characterized by $D > 0$ and oblate spheroidal shapes by $D < 0$.

3. Small deformation analysis – analytic solution

In this section, we use the established method of domain perturbations to outline an analytic solution for the velocity and pressure fields internal and external to a compound multiphase drop that is immersed in a general linear flow field. The results of the analysis are summarized in §4. In order to make analytical progress, the drops comprising the double emulsion globule are treated as concentric, in the sense that their centres of mass are coincident, and their shapes are treated as nearly spherical. In the domain perturbation procedure, the velocity field is calculated everywhere using the continuity of velocity and continuity of tangential stress boundary conditions at the undeformed, spherical interfaces. This produces the first term in an asymptotic expansion for the velocity field based upon a small drop deformation. The resulting flow generates viscous stresses that tend to deform the globule and the normal stress balance is used to determine a first approximation to the perturbed steady-state shape.

The basic assumption in the analysis reported in this section is that the inner and outer drops remain nearly spherical. There are two independent limits where a drop will remain nearly spherical. The first is low capillary number (in other words, weak flows or large interfacial tensions) and the second is a large internal viscosity. We will deal principally with the low $\mathbb{C}$ case.

The most general form of the solution to Stokes equation is given by Lamb (1932) in terms of an expansion in spherical harmonics. Lamb's general solution is particularly well-suited to problems with spherical symmetry and has been applied to the related problem of single-phase drop deformation by Taylor (1932), Cox (1969), Frankel & Acrivos (1970), Barthès-Biesel & Acrivos (1973*a*) and Rallison (1980). We follow a similar procedure here, although we are content with only the leading-order approximation for the general case $\lambda_{21} = O(1)$ and $\lambda_{32} = O(1)$. This provides good physical insight and motivates the numerical simulations discussed in §6.

As a result of the assumption of small deformation, both the governing equations and the applicable boundary conditions are linear. Since the droplets are assumed concentric and the undisturbed fluid motion is characterized by the second-order tensor $\boldsymbol{\Gamma}$, the velocity and pressure fields in the suspending fluid (phase 1: $r = |\boldsymbol{x}| \geqslant 1$) may be written in the following general form:

$$\boldsymbol{u}_1(\boldsymbol{x}) = \boldsymbol{E}\cdot\boldsymbol{x} + \tfrac{1}{2}\boldsymbol{\omega}\wedge\boldsymbol{x} + \tfrac{1}{2}B_1\boldsymbol{x}\frac{\boldsymbol{x}\cdot\boldsymbol{E}\cdot\boldsymbol{x}}{r^5} + \frac{C_1}{r^5}\left[2\boldsymbol{E}\cdot\boldsymbol{x} - 5\boldsymbol{x}\frac{\boldsymbol{x}\cdot\boldsymbol{E}\cdot\boldsymbol{x}}{r^2}\right] + \frac{D_1\boldsymbol{\omega}\wedge\boldsymbol{x}}{r^3}, \quad (7a)$$

$$p_1(\boldsymbol{x}) = p_\infty + \frac{B_1\boldsymbol{x}\cdot\boldsymbol{E}\cdot\boldsymbol{x}}{r^5}. \quad (7b)$$

The external flow, represented by $\boldsymbol{E}$ and $\boldsymbol{\omega}$, is prescribed and the last three terms on the right-hand side of equation (7*a*) represent the disturbance motion caused by the globule and decay as $|\boldsymbol{x}| \to \infty$.

The velocity and pressure fields in the inner droplet (phase 3: $|\boldsymbol{x}| \leqslant \kappa$) must remain bounded as $r \to 0$ and have the general form

$$\boldsymbol{u}_3(\boldsymbol{x}) = 2F_3 \boldsymbol{E}\cdot\boldsymbol{x} + G_3 \boldsymbol{\omega}\wedge\boldsymbol{x} + \frac{H_3 r^2}{21}\left[5\boldsymbol{E}\cdot\boldsymbol{x} - 2\boldsymbol{x}\frac{\boldsymbol{x}\cdot\boldsymbol{E}\cdot\boldsymbol{x}}{r^2}\right], \tag{8a}$$

$$p_3(\boldsymbol{x}) = p_3^* + H_3 \boldsymbol{x}\cdot\boldsymbol{E}\cdot\boldsymbol{x}. \tag{8b}$$

In the annular region (phase 2: $\kappa \leqslant |\boldsymbol{x}| \leqslant 1$), spherical harmonics of both positive and negative degree are necessary so that

$$\boldsymbol{u}_2(\boldsymbol{x}) = 2F_2 \boldsymbol{E}\cdot\boldsymbol{x} + G_2 \boldsymbol{\omega}\wedge\boldsymbol{x} + \tfrac{1}{2}B_2 \boldsymbol{x}\left(\frac{\boldsymbol{x}\cdot\boldsymbol{E}\cdot\boldsymbol{x}}{r^5}\right) + \frac{C_2}{r^5}\left[2\boldsymbol{E}\cdot\boldsymbol{x} - 5\boldsymbol{x}\frac{\boldsymbol{x}\cdot\boldsymbol{E}\cdot\boldsymbol{x}}{r^2}\right] + \frac{D_2 \boldsymbol{\omega}\wedge\boldsymbol{x}}{r^3} + \frac{H_2 r^2}{21}\left[5\boldsymbol{E}\cdot\boldsymbol{x} - 2\boldsymbol{x}\frac{\boldsymbol{x}\cdot\boldsymbol{E}\cdot\boldsymbol{x}}{r^2}\right], \tag{9a}$$

$$p_2(\boldsymbol{x}) = p_2^* + \frac{B_2 \boldsymbol{x}\cdot\boldsymbol{E}\cdot\boldsymbol{x}}{r^5} + H_2 \boldsymbol{x}\cdot\boldsymbol{E}\cdot\boldsymbol{x}. \tag{9b}$$

In these equations, p_2^* and p_3^* are constant pressure terms which are related to p_∞ and the curvature of the undeformed spherical interfaces. The corresponding stress fields are straightforward to calculate and are listed for completeness in Appendix B.

The drop shape is approximated by an expansion in surface spherical harmonics, where we retain, at leading order, only the second-order term since the flow field is described by a second-order tensor (Rallison 1980) (the zero- and first-order harmonics correspond to translation and dilatation of the drop only, Cox 1969). Hence, the shapes of the fluid–fluid interfaces are assumed to be of the form

$$r = 1 + \frac{A_{21}\boldsymbol{x}\cdot\boldsymbol{E}\cdot\boldsymbol{x}}{r^2} \quad \text{for } \boldsymbol{x}_s \in S_{21}, \tag{10a}$$

$$r = \kappa\left[1 + \frac{A_{32}\boldsymbol{x}\cdot\boldsymbol{E}\cdot\boldsymbol{x}}{r^2}\right] \quad \text{for } \boldsymbol{x}_s \in S_{32}. \tag{10b}$$

The coefficients A_{21} and A_{32}, which describe the magnitude of the leading-order shape correction, must be determined as part of the solution to the problem. Equation (10) emphasizes the fact that the steady drop deformation, at the leading-order approximation, depends only on the rate-of-strain tensor $\boldsymbol{E}$ and is independent of the vorticity. Clearly, for this small deformation analysis to be valid, the magnitudes of both A_{21} and A_{32} must be small. We will make this qualitative statement more precise below. Higher-order harmonics would appear in (10) if additional terms in an asymptotic expansion for the velocity field were desired. These higher-order terms have been calculated for the single-phase drop problem by Barthès-Biesel & Acrivos (1973*a*), but the algebra was very complicated and required the use of a computer. We are content here to calculate the leading-order term in order to develop physical insight about the velocity field and the small deformation produced by the viscous stresses and then use the numerical analysis to study finite deformations.

If we define the shape function as

$$f_{21} = r - \left[1 + \frac{A_{21}\boldsymbol{x}\cdot\boldsymbol{E}\cdot\boldsymbol{x}}{r^2}\right] = \text{constant} = 0,$$

then the unit outward normal to the outer interface can be calculated from

$$\boldsymbol{n}_2 = \frac{\nabla f_{21}}{|\nabla f_{21}|}.$$

It follows that the local mean curvature of the slightly deformed outer surface is given by

$$\nabla_s \cdot \boldsymbol{n}_2 = 2 + 4A_{21}\, \boldsymbol{n}_2^\circ \cdot \boldsymbol{E} \cdot \boldsymbol{n}_2^\circ, \tag{11a}$$

where the superscript $^\circ$ denotes the normal to the spherical surface. Similarly for the inner surface we have

$$\nabla_s \cdot \boldsymbol{n}_3 = \frac{1}{\kappa}\left[2 + 4A_{32}\, \boldsymbol{n}_3^\circ \cdot \boldsymbol{E} \cdot \boldsymbol{n}_3^\circ\right]. \tag{11b}$$

Following standard procedures of the domain perturbation technique, the $O(1)$ velocity field is calculated by applying continuity of velocity, continuity of tangential stress, and the kinematic condition on the undeformed spherical surfaces ($\boldsymbol{x}_s = \boldsymbol{n}_2^\circ, r = 1$ on S_{21} and $\boldsymbol{x}_s = \kappa \boldsymbol{n}_3^\circ, r = \kappa$ on S_{32}). The normal stress balance is then used to calculate the first correction to the drop shape. Further details for the solution of this problem may be found in Appendix A. Using this solution the equations for the shape functions A_{21} and A_{32} may be expressed in the form

$$\left.\begin{aligned} A_{21} &= \tfrac{1}{4}\mathbb{C}_0 h_{21}(\kappa, \lambda_{21}, \lambda_{32}), \\ A_{32} &= \frac{\mathbb{C}_0 \lambda_{21} \kappa}{4\Omega} h_{32}(\kappa, \lambda_{21}, \lambda_{32}) = \tfrac{1}{4}\mathbb{C}_1 h_{32}. \end{aligned}\right\} \tag{12}$$

The functions h_{21} and h_{32} are also listed in Appendix A. The form of the solutions (12) confirms the requirements, $\mathbb{C}_0 \ll 1$ and $\mathbb{C}_1 \ll 1$ for validity of the small deformation analysis for $\lambda_{21} = O(1)$ and $\lambda_{32} = O(1)$. It is evident from (10) and (12) that both drops initially deform into ellipsoids when these conditions are satisfied. Although the time evolution of the shape functions A_{21} and A_{32} could be determined by using the complete form of the kinematic conditions (6), rather than $\boldsymbol{n} \cdot \boldsymbol{u} = 0$, this is algebraically tedious and is not attempted here. Instead, we will illustrate the time-dependent evolution of the interfaces for finite deformation using the numerical simulations discussed in §6.

Before discussing the details of the approximate solution from this section, we note that it can be used to determine the effective viscosity of a dilute suspension of spherical double emulsion droplets. The analysis of the bulk stress in a dilute suspension of particles has been discussed by Batchelor (1970). The bulk stress, $\boldsymbol{\Sigma}$, is related to the rate-of-strain tensor $\boldsymbol{E}$ by

$$\boldsymbol{\Sigma} = -p\boldsymbol{I} + 2\boldsymbol{E} + \boldsymbol{\Sigma}^{(\mathrm{p})}, \tag{13}$$

where

$$\boldsymbol{\Sigma}^{(\mathrm{p})} = \frac{3\phi}{4\pi}\int_{S_{21}} [(\boldsymbol{T}_1 \cdot \boldsymbol{n}_2)\, \boldsymbol{x} - (\boldsymbol{u}_1 \boldsymbol{n}_2 + \boldsymbol{n}_2 \boldsymbol{u}_1)]\, \mathrm{d}S, \tag{14}$$

represents the contribution to the bulk stress due to the presence of the particles. Here, ϕ is the particle volume fraction and the integration is over the outer surface of the globule. Because the solution presented above treats the globule as spherical, it is straightforward to show that the only contribution to this integral comes from the B_1 term of the solution. Hence,

$$\boldsymbol{\Sigma}^{(\mathrm{p})} = -\phi B_1 \boldsymbol{E}, \tag{15}$$

so that a dilute emulsion of concentric spherical droplets behaves as a Newtonian fluid with an effective viscosity, μ^*, given by

$$\frac{\mu^*}{\mu} = 1 + \phi B_1(\kappa, \lambda_{21}, \lambda_{32}). \tag{16}$$

The magnitude of the capillary number plays no role at this level of approximation. Globule deformation, which depends on both the magnitude of the capillary number and the flow type, leads to more complicated rheological properties (e.g. normal stress differences). This has been discussed for a dilute suspension of single-phase droplets by Schowalter, Chaffey & Brenner (1968), Frankel & Acrivos (1970) and Barthès-Biesel & Acrivos (1973*b*).

4. Small deformation analysis – results

We begin our discussion of the analytical results by illustrating typical streamlines internal and external to the globule. In figure 2 we exhibit the streamline patterns for $\kappa = 0.2$ and 0.8. The other parameters are fixed at $\lambda_{21} = 1.0, \lambda_{32} = 1.0$. As Ω and $\mathbb{C}_0$ appear only in the normal stress balance, they play a role in the deformation of the interfaces, but do not effect the velocity field at this order of approximation. The arrows on the streamlines shown in figure 2 correspond to the case of a uniaxial extensional flow. However, because of the assumptions of spherical and concentric drops, the streamline patterns are identical for uniaxial or biaxial extensional flows; only the direction of flow is reversed in these two cases.

In figure 2, we observe two vortical flow patterns interior to the globule. The important point to notice is that the external fluid motion creates a recirculating flow in the annular region that drives a flow in the inner droplet with an opposite sense of rotation. The effect of changing λ_{21} and λ_{32} was examined and found to have very little qualitative effect on the streamline pattern with the change limited to the magnitude of the velocity.

The streamline patterns shown in figure 2 suggest an interesting feature of the flow-induced deformation of the globule. The external *uniaxial* flow will tend to deform the overall globule into a prolate spheroidal shape. Meanwhile, the steady interior flow generated in the annular region creates a *biaxial* extensional flow in the neighbourhood of the inner droplet. This deforms the inner droplet into an oblate spheroidal shape. Exactly the reverse situation would occur if a biaxial extensional flow were imposed at infinity: the overall globule would deform into an oblate ellipsoid, but the inner droplet would be exposed to a uniaxial extensional flow and thus deform into a prolate ellipsoid. A typical series of steady-state shapes is shown as a function of capillary number in figure 3 for a globule immersed in a uniaxial extensional flow. The results for the corresponding biaxial extensional flow are shown in figure 4. The final shapes shown in figures 3 and 4 have both developed a pinch at the droplet centre. This may not be physically correct, as it may occur because the asymptotic solution is being used outside its range of validity and numerical methods must be used to address these large distortions. For small deformations, the magnitude of deformation of both the inner and outer droplet increases linearly with capillary number (equation (12)). Furthermore, the deformation of the inner droplet is much smaller than the deformation of the outer droplet. Of course, the basic reason for this is that the smaller radius of curvature of the inner droplet makes interfacial tension more important, i.e. $\mathbb{C}_1 = \mathbb{C}_0 \kappa \lambda_{21} / \Omega$. Finally, this simultaneous existence of prolate shapes containing flow-induced oblate shapes, and vice versa, is similar

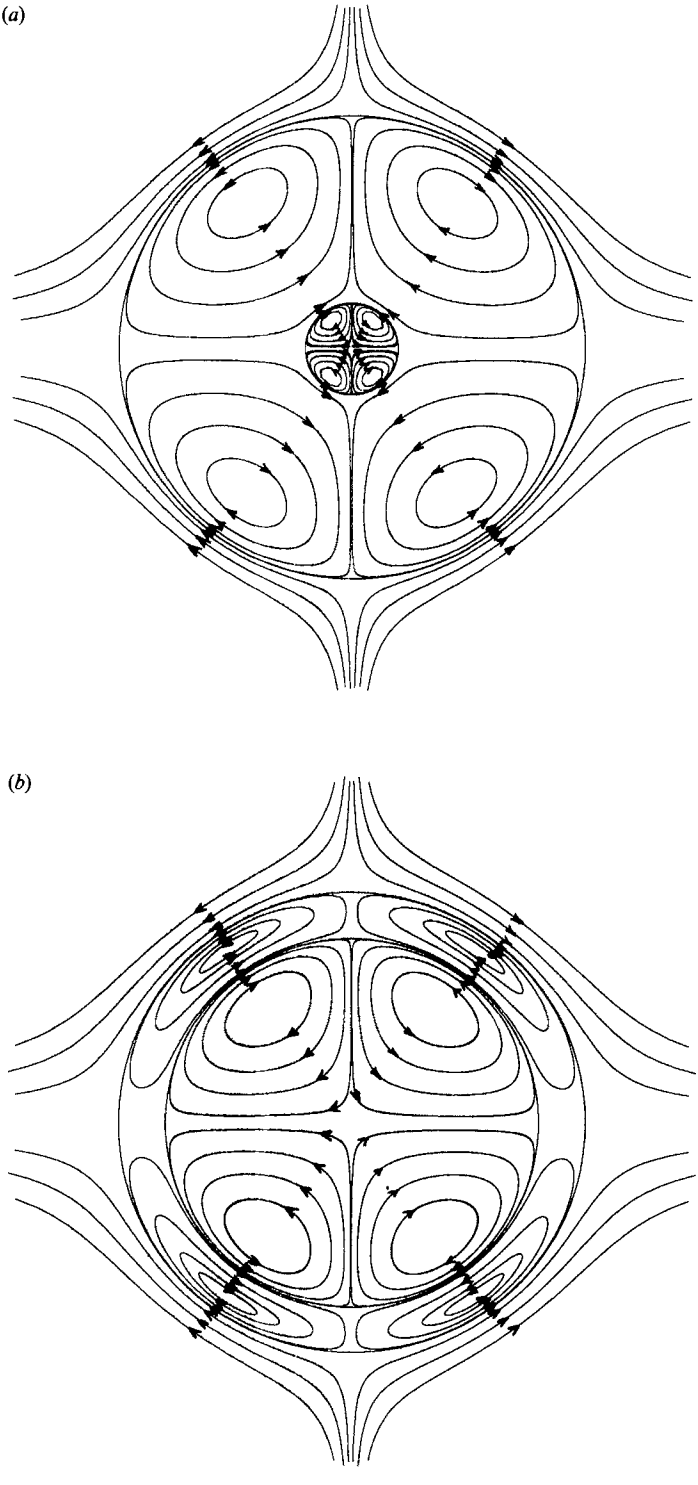

FIGURE 2. Streamlines in and around the compound droplet as a function of the internal droplet size, $\lambda_{21} = \lambda_{32} = 1.0$ (*A*) $\kappa = 0.2$; (*b*) $\kappa = 0.8$.

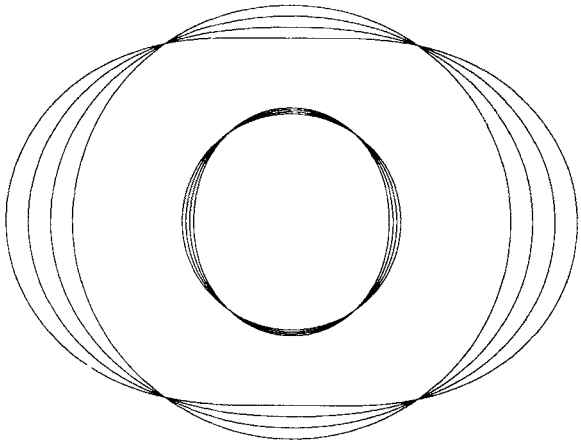

FIGURE 3. Deformation of a double emulsion droplet in a uniaxial extensional flow; $\mathbb{C}_o = 0, 0.04, 0.08, 0.12$.

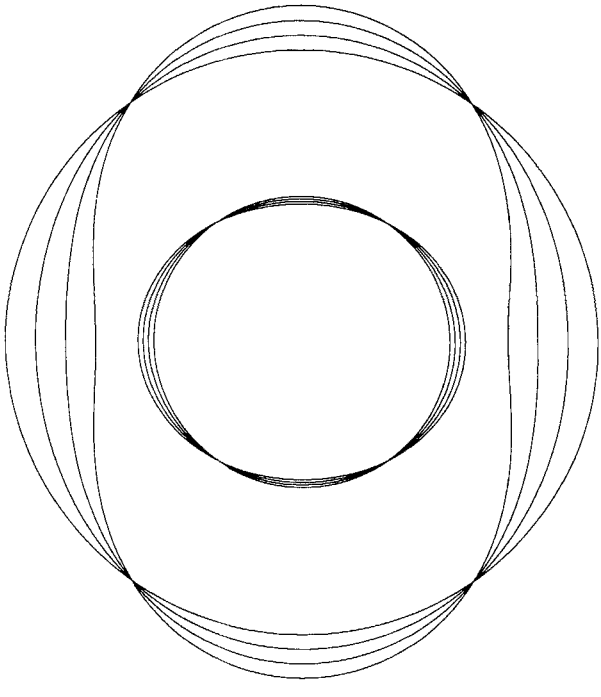

FIGURE 4. Deformation of a double emulsion droplet in a biaxial extensional flow; $\mathbb{C}_o = 0, 0.04, 0.08, 0.12$.

qualitatively to observations of Brunn & Roden (1985), Chervenivanova & Zapryanov (1988) and Tsamapoulos & Brown (1987), even though the base-flow situations are very different.

It is well-established that the critical capillary number for drop breakup is dependent on the nature of the flow field. For example, in the single-phase case, drops of any viscosity ratio can be burst in a steady two-dimensional extensional flow. However, for steady simple shear flow there exists a limiting value of the viscosity

ratio above which breakup does not occur. Furthermore, even the nature of an extensional flow (uniaxial versus biaxial) can lead to differences in the breakup of single-phase droplets. Small deformation studies of single-phase droplets in biaxial and uniaxial extensional flows have been performed by Barthès-Biesel & Acrivos (1973*a*) and a numerical study of finite deformation of droplets at zero Reynolds number in both biaxial and uniaxial flows is presented by Stone & Leal (1989 *a*, *b*). The most notable feature regarding breakup at low Reynolds numbers is that the critical capillary number for non-existence of steady solutions (i.e. 'burst') is larger in a biaxial flow. This is particularly relevant to this study where one drop experiences a uniaxial straining flow, while simultaneously the other drop experiences a biaxial straining flow. Although a complete investigation of the conditions for breakup of globules must await the finite deformation numerical study in §4, the small deformation analysis does provide useful qualitative insight.

In particular, one question that we can consider is the effect that the presence of the inner droplet has on the overall deformation of the globule. In figure 5 we present a plot of the globule deformation, D_{outer}, versus capillary number for four different radius ratios, $\kappa = 0.1, 0.3, 0.5$ and 0.7. The curve for $\kappa = 0.7$ stops when the analysis predicts that the inner and outer interfaces touch. The other parameters are fixed at the values $\lambda_{21} = 1.0, \lambda_{32} = 1.0$ and $\Omega = 1.0$. Although this plot is extended to include finite deformation, we do not expect that the present analysis will provide more than a qualitative indication of the dependence of deformation on capillary number and κ for such cases. Clearly, however, the effect of increasing κ is to significantly increase the deformation of the outer interface at a given value of the capillary number. This result is in agreement with the work of Davis & Brenner (1981), who observed that in a simple shear flow, the effect of increasing the size of an occluded rigid particle was to increase the droplet deformation. This suggests that breakup with the occluded phase present may occur at a reduced value of the capillary number. However, it should be remarked that the inner droplet deforms toward the narrowing waist of the outer droplet (cf. figures 3 and 4), so that significant hydrodynamic interactions between the two interfaces will occur. This interaction between the two fluid–fluid interfaces, a result of finite deformation, is not taken into account in the small-deformation theory. As a consequence, a definitive conclusion about the effect of the third phase on conditions for breakup is not possible on the basis of the small deformation alone. This question must be answered via a numerical investigation including finite deformation (§§5–6).

Next we examine the effect of varying the fluid properties. As is clear from (12), the ratio of interfacial tensions Ω in this small deformation limit only influences the deformation of the inner droplet and has no effect on deformation on the overall globule. In effect, variation of Ω is equivalent to changes in the capillary number for the inner drop, $\mathbb{C}_i$. Hence for a given outer capillary number $\mathbb{C}_o$, more deformation of the inner droplet occurs for smaller Ω and larger κ.

The effect of changing the viscosity of the occluded phase is examined in figure 6 by varying λ_{32}, for fixed $\lambda_{21} = 1.0, \Omega = 1.0$ and $\kappa = 0.5$. In figure 6(*a*), the deformations of the outer globule and inner drop are shown as a function of the capillary number $\mathbb{C}_o$ by the solid and dashed lines, respectively, and in this case $\mathbb{C}_i = 0.5\mathbb{C}_o$. It can be seen that the deformation of both drops increases slightly with increase of $\lambda_{32} > 0.1$. The increased deformation of the inner drop as the viscosity of the encapsulated phase is increased is in agreement with previous experiments and small-deformation studies of single-phase drops, which show that for $\lambda > O(1)$, deformation increases as the viscosity ratio increases. In figure 6(*b*) we show similar

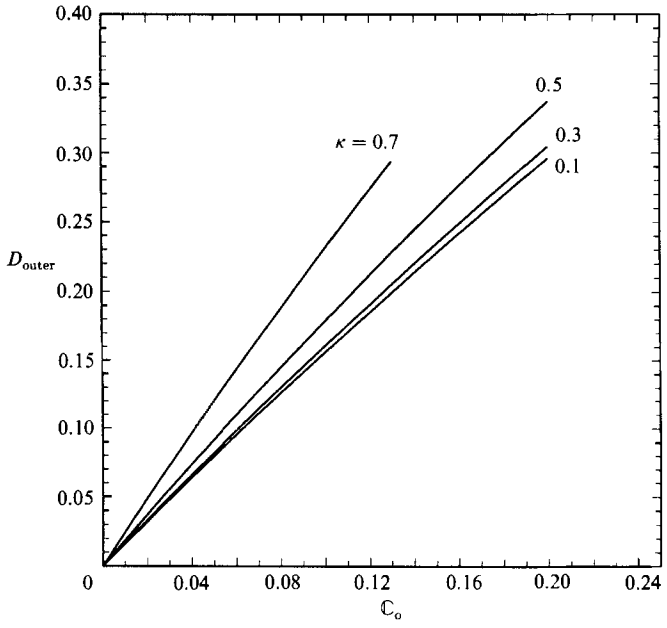

FIGURE 5. Overall globule deformation D_{outer} as a function of capillary number. $K = 0.1, 0.3, 0.5$ and 0.7. The $\kappa = 0.7$ curve is stopped when the analysis predicts that the interfaces overlap.

calculations for $\kappa = 0.1$. For this small encapsulated particle, the deformation of the globule is effectively independent of the viscosity of the occluded phase as values of D_{outer} differ by less than 1% for $10^{-2} \leqslant \lambda_{32} \leqslant 10^2$. The inner drop is barely deformed since the inner capillary number is always very small, $\mathbb{C}_i = 0.1\mathbb{C}_o$.

For completeness, we also examine the effect of varying λ_{21} for two cases $\kappa = 0.5$ and $\kappa = 0.1$ as shown in figure 7. For fixed values of λ_{32} and $\mathbb{C}_o$, increasing λ_{21} is equivalent to increasing μ_2 and μ_3 by the same amount. This has the effect of increasing the capillary number for the inner drop, $\mathbb{C}_i = \mathbb{C}_o \lambda_{21} \kappa / \Omega$. Thus, the effect of increasing λ_{21} is to slightly increase the degree of globule deformation by effectively making the inner medium more viscous, as well as significantly increasing the deformation of the inner drop by increasing $\mathbb{C}_i$. Nevertheless, at a given $\mathbb{C}_i$, the degree of deformation of the inner drop is smaller than that of the equivalent outer drop at a given $\mathbb{C}_o$, which implies that the characteristic velocity chosen to define $\mathbb{C}_i$ is not simply G but presumably depends on λ_{21}. This is also evident by examining the deformation curves for the inner drop at different λ_{21}.

If we combine all of the above results and assume that increased deformation of the globule leads to breakup at a lower value of the capillary number, then the conclusion from figures 5, 6 and 7 is that breakup is enhanced when the size of the interior drop is increased or the interior fluids are more viscous. Whether these conclusions will carry over to finite deformation remains to be seen and will be examined in §6.

Finally, we present a brief discussion of the rheology to be expected of a dilute emulsion of multiphase globules. The contribution to the bulk stress because of the presence of particles is summarized in §3. Following the notation of Davis & Brenner (1981), the bulk viscosity, μ^* can be written in the form

$$\frac{\mu^*}{\mu} = 1 + \tfrac{5}{2}\phi(1 - \tfrac{3}{5}K), \tag{17}$$

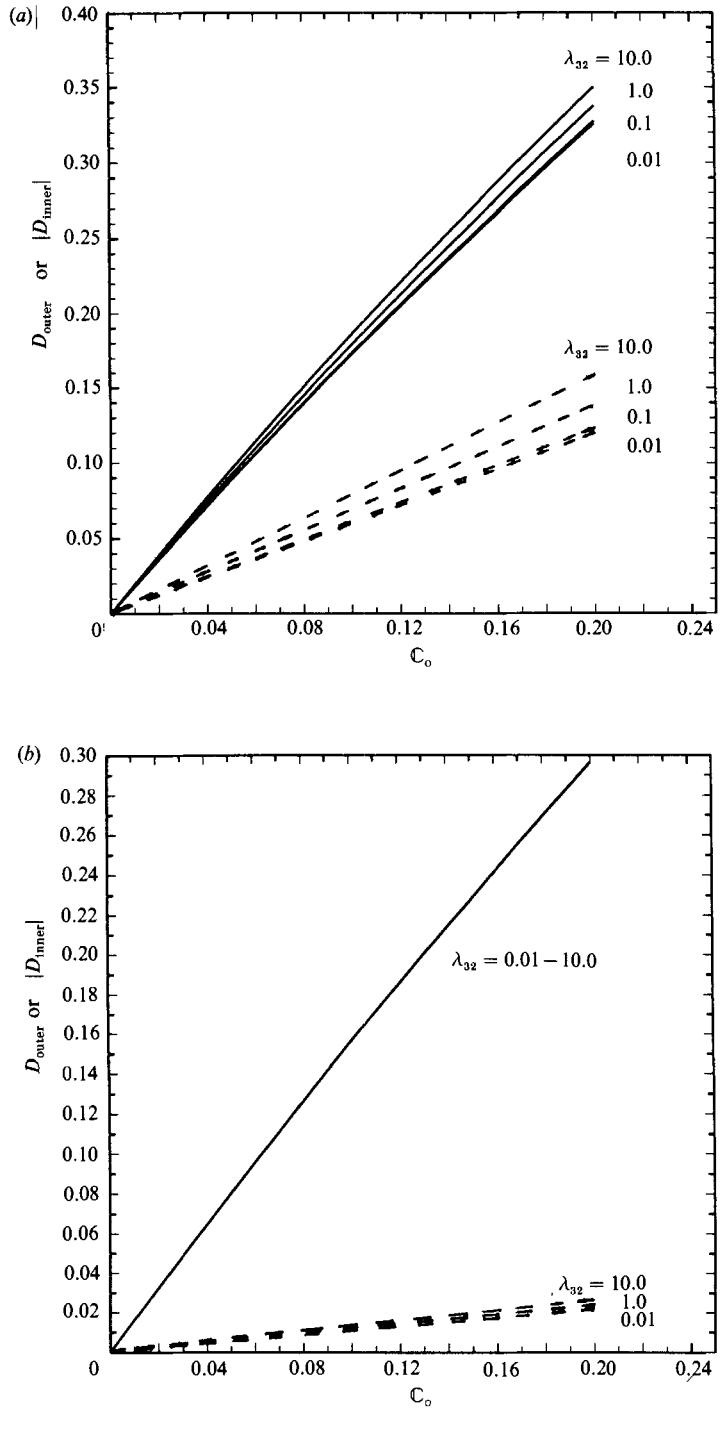

FIGURE 6. Deformation of the inner (dashed line) and outer (solid line) droplets due to varying λ_{32}. $\lambda_{21} = 1.0$, $\Omega = 1.0$. (*a*) $\kappa = 0.5$; (*b*) $\kappa = 0.1$.

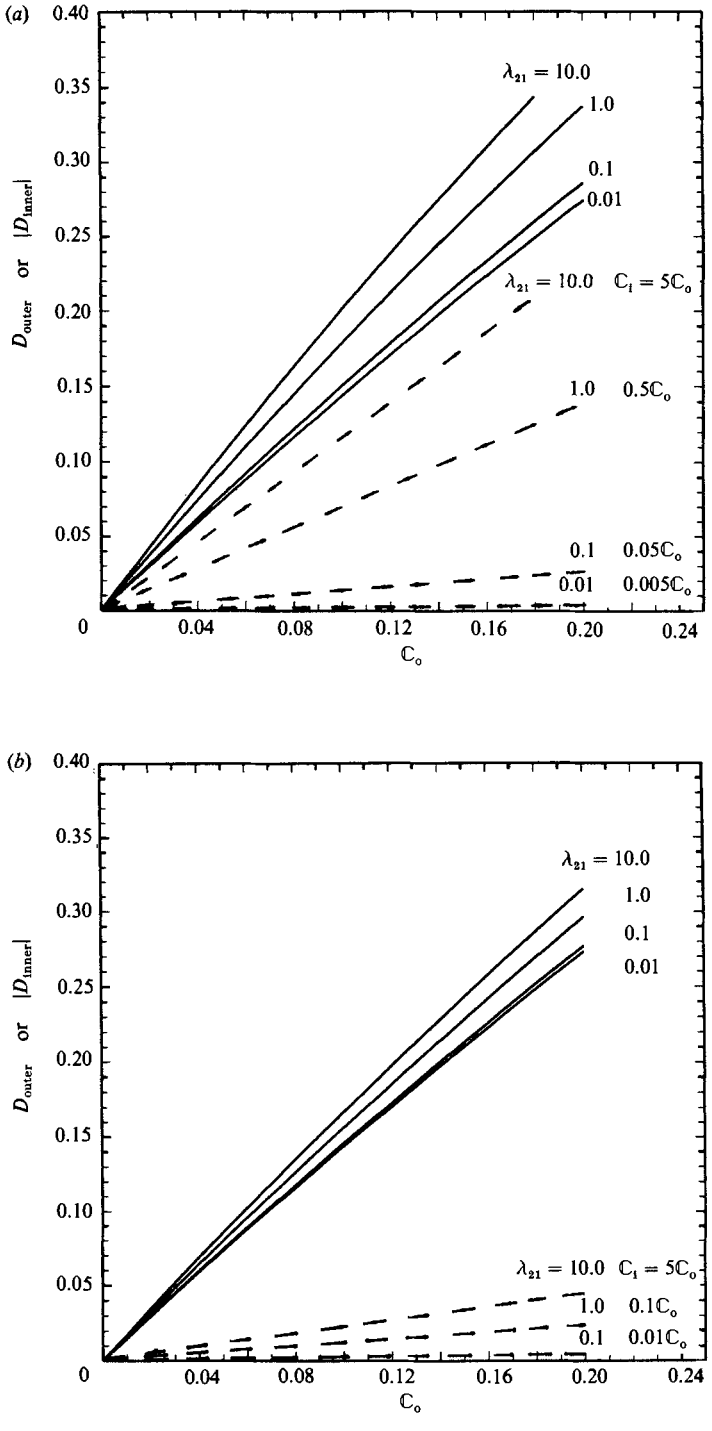

FIGURE 7. Deformation of the inner (dashed line) and outer (solid line) droplets due to varying λ_{21}. $\lambda_{32} = 1.0$, $\Omega = 1.0$. (*a*) $\kappa = 0.5$; (*b*) $\kappa = 0.1$.

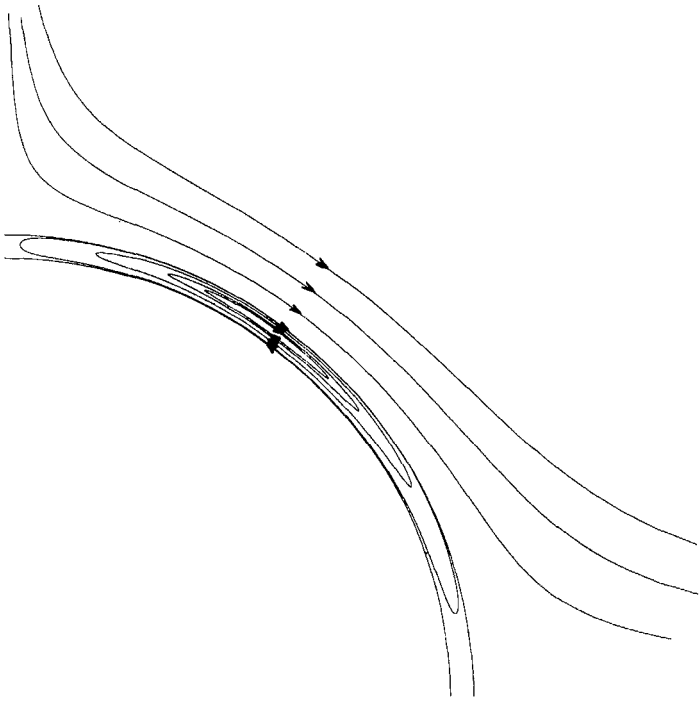

FIGURE 8. The velocity profile in the annular region of the globule in the limit $\kappa \to 1.0$. $\kappa = 0.95$. The boundary of the globule acts effectively as a no-slip surface in this limit so that a dilute emulsion of these droplets behaves as a suspension of rigid spheres.

where
$$K = \frac{\delta_1 + \dfrac{\kappa^3}{1+\lambda_{32}}\delta_2}{\delta_1 + \lambda_{21}\delta_3 + \dfrac{\kappa^3}{1+\lambda_{32}}(\delta_2 + \lambda_{21}\delta_4)}. \tag{18}$$

The coefficients δ_i only depend on κ and have the specific forms

$$\delta_1 = 4 - 25\kappa^3 + 42\kappa^5 - 25\kappa^7 + 4\kappa^{10},$$
$$\delta_2 = 15 - 42\kappa^2 + 35\kappa^4 - 8\kappa^7,$$
$$\delta_3 = 4 - 10\kappa^3 + 10\kappa^7 - 4\kappa^{10},$$
$$\delta_4 = 6 - 14\kappa^4 + 8\kappa^7.$$

In the limit $\lambda_{32} \to \infty$ (λ_{21} and κ finite) this expression reduces to the result of Davis & Brenner (1981) for a solid sphere occluded at the globule centre. As discussed by Davis & Brenner, two other limits follow naturally. In the limit $\lambda_{21} \to \infty$, the case of a very viscous shell of fluid, equation (30) yields $K \to 0$, which is the well-known Einstein viscosity for a suspension of solid spheres. Notice that this is true for any κ and λ_{32} and simply says that the interior fluid plays no part in the rheology if the liquid membrane, however thin, is much more viscous than the suspending fluid. The effect of the viscous membrane is to reduce the velocity in the annular region to $O(1/\lambda_{21})$ so that the effective deformation rate in the neighbourhood of the inner drop

is very small. The limit $\kappa \to 0$ reproduces the results of Taylor (1932) for the viscosity of a suspension of single-phase liquid droplets

$$\frac{\mu^*}{\mu} = 1 + \phi \frac{1 + \frac{5}{2}\lambda_{21}}{1 + \lambda_{21}}.$$

Another interesting limit is found by considering the case of a very thin liquid membrane, $\kappa \to 1$. In this case we find

$$K = \frac{175\bar{\kappa}^2 + \dfrac{\bar{\kappa}}{1+\lambda_{32}}(140 - 665\bar{\kappa})}{175\bar{\kappa}^2 + \bar{\kappa}\lambda_{21}(140 - 490\bar{\kappa}) + \dfrac{1}{1+\lambda_{32}}[140\bar{\kappa} + \lambda_{21}(84 - 476\bar{\kappa})]} + O[(\bar{\kappa}^3)],$$

where $\bar{\kappa} = 1 - \kappa$. Hence, provided $\lambda_{21} = O(1)$ the limit $\kappa \to 1$ ($\bar{\kappa} \to 0$) produces $K \to 0$, which is the result for a suspension of rigid spheres. This dynamic property of thin liquid membranes to reproduce solid sphere-like rheological behaviour is best appreciated by examining the velocity field. In figure 8 we show a magnified view of the fluid streamlines for $\kappa = 0.95$. Because of the recirculation set up internal to the droplet, the fluid velocity is forced to change directions over a very short distance. In order to satisfy continuity of velocity at both interfaces, the tangential velocity is reduced to zero, as it would be at a solid boundary. Therefore, the viscosity is equivalent to a suspension of rigid spheres. This result is independent of the viscosity of the inner phase. The equivalent consequence of thin membranes for sedimenting double emulsion droplets was pointed out by Rushton & Davies (1983).

5. Numerical study of finite deformation: application of the boundary integral method

Although the analysis presented above provides insight and is straightforward, it is nonetheless restricted to small deformations. The effect of large deformations and the possibility of breakup are clearly interesting and significant problems. However, as is characteristic of most free-boundary problems, the study of large deformations is amenable only to numerical study. A powerful method for solving Stokes flow problems is the boundary integral method (Youngren & Acrivos 1975). The technique has been applied to several aspects of the single-phase drop deformation problem (Rallison & Acrivos 1978; Rallison 1980; Stone & Leal 1989*a*), in addition to a variety of other free-boundary studies (Lee & Leal 1982; Sherwood 1988; Stoos & Leal 1989).

The governing equations and boundary conditions are outlined in §2. The general solution to the quasi-steady Stokes equation in the three phases may be written as

$$\boldsymbol{u}_i(\boldsymbol{x}) = \boldsymbol{u}_\infty(\boldsymbol{x}) + \int_S \boldsymbol{J}\cdot\boldsymbol{T}_i\cdot\boldsymbol{n}_i \,\mathrm{d}S(\boldsymbol{y}) + \int_S \boldsymbol{u}_i\cdot\boldsymbol{K}\cdot\boldsymbol{n}_i \,\mathrm{d}S(\boldsymbol{y}), \tag{19}$$

where S represents all the bounding surfaces for phase i, $\boldsymbol{n}_i$ is the unit outward normal from phase i (see figure 1), and $\boldsymbol{u}_\infty = 0$ for phase 2 and phase 3. In this equation the kernels $\boldsymbol{J}$ and $\boldsymbol{K}$ are defined as

$$\boldsymbol{J}(\boldsymbol{x}-\boldsymbol{y}) = \frac{1}{8\pi}\left[\frac{\boldsymbol{I}}{|\boldsymbol{x}-\boldsymbol{y}|} + \frac{(\boldsymbol{x}-\boldsymbol{y})(\boldsymbol{x}-\boldsymbol{y})}{|\boldsymbol{x}-\boldsymbol{y}|^3}\right],$$

$$\boldsymbol{K}(\boldsymbol{x}-\boldsymbol{y}) = -\frac{3}{4\pi}\frac{(\boldsymbol{x}-\boldsymbol{y})(\boldsymbol{x}-\boldsymbol{y})(\boldsymbol{x}-\boldsymbol{y})}{|\boldsymbol{x}-\boldsymbol{y}|^5}.$$

We proceed by taking the limit of (19) as $\boldsymbol{x} \to \boldsymbol{x}_s \in S_{21}$ from phase 1 and phase 2, respectively. Making use of the continuity of the single layer and the jump condition for the double layer (Ladyzhenskaya 1969), thus results in the two equations

$$\tfrac{1}{2}\boldsymbol{u}_1(\boldsymbol{x}_s) = \boldsymbol{u}_\infty(\boldsymbol{x}_s) - \int_{S_{21}} \boldsymbol{J}\cdot\boldsymbol{T}_1\cdot\boldsymbol{n}_2\,\mathrm{d}S - \int_{S_{21}} \boldsymbol{u}_1\cdot\boldsymbol{K}\cdot\boldsymbol{n}_2\,\mathrm{d}S, \tag{20}$$

$$\tfrac{1}{2}\boldsymbol{u}_2(\boldsymbol{x}_s) = \int_{S_{21}} \boldsymbol{J}\cdot\boldsymbol{T}_2\cdot\boldsymbol{n}_2\,\mathrm{d}S + \int_{S_{32}} \boldsymbol{J}\cdot\boldsymbol{T}_2\cdot\boldsymbol{n}_2\,\mathrm{d}S + \int_{S_{21}} \boldsymbol{u}_2\cdot\boldsymbol{K}\cdot\boldsymbol{n}_2\,\mathrm{d}S + \int_{S_{32}} \boldsymbol{u}_3\cdot\boldsymbol{K}\cdot\boldsymbol{n}_2\,\mathrm{d}S. \tag{21}$$

These equations are valid for $\boldsymbol{x}_s \in S_{21}$. The integrands in the integrals over S_{21} are singular, but the integrals themselves are integrable in the sense of a Cauchy principal value. The integrals over S_{32} are non-singular.

Multiplying (21) by λ_{21}, adding to (20) and making use of the boundary conditions on the velocity and stress fields at the S_{21} surface gives

$$\tfrac{1}{2}(1+\lambda_{21})\,\boldsymbol{u}_1(\boldsymbol{x}_s) = \boldsymbol{u}_\infty(\boldsymbol{x}_s) - \frac{1}{\mathbb{C}_0}\int_{S_{21}} \boldsymbol{J}\cdot\boldsymbol{n}_2(\nabla_s\cdot\boldsymbol{n}_2)\,\mathrm{d}S - (1-\lambda_{21})\int_{S_{21}} \boldsymbol{u}_1\cdot\boldsymbol{K}\cdot\boldsymbol{n}_2\,\mathrm{d}S + \lambda_{21}\int_{S_{32}} \boldsymbol{J}\cdot\boldsymbol{T}_2\cdot\boldsymbol{n}_2\,\mathrm{d}S + \lambda_{21}\int_{S_{32}} \boldsymbol{u}_3\cdot\boldsymbol{K}\cdot\boldsymbol{n}_2\,\mathrm{d}S. \tag{22}$$

This equation describes the velocity $\boldsymbol{u}_1$ at the S_{21} interface in terms of integrals over both interfaces. Unlike the single-phase droplet deformation problem where only the surface curvature $\nabla_s\cdot\boldsymbol{n}$ is necessary to determine the interface evolution (Rallison & Acrivos 1978), in this multiphase droplet problem the velocity and stress on the second interface are needed also.

In a similar manner, taking the limit of (19) as $\boldsymbol{x} \to \boldsymbol{x}_s \in S_{32}$ from phase 2 and phase 3 results in the two equations

$$\tfrac{1}{2}\boldsymbol{u}_2(\boldsymbol{x}_s) = \int_{S_{21}} \boldsymbol{J}\cdot\boldsymbol{T}_2\cdot\boldsymbol{n}_2\,\mathrm{d}S + \int_{S_{32}} \boldsymbol{J}\cdot\boldsymbol{T}_2\cdot\boldsymbol{n}_2\,\mathrm{d}S + \int_{S_{21}} \boldsymbol{u}_2\cdot\boldsymbol{K}\cdot\boldsymbol{n}_2\,\mathrm{d}S + \int_{S_{32}} \boldsymbol{u}_2\cdot\boldsymbol{K}\cdot\boldsymbol{n}_2\,\mathrm{d}S, \tag{23}$$

$$\tfrac{1}{2}\boldsymbol{u}_3(\boldsymbol{x}_s) = -\int_{S_{32}} \boldsymbol{J}\cdot\boldsymbol{T}_3\cdot\boldsymbol{n}_3\,\mathrm{d}S - \int_{S_{32}} \boldsymbol{u}_3\cdot\boldsymbol{K}\cdot\boldsymbol{n}_3\,\mathrm{d}S. \tag{24}$$

Multiplying (24) by λ_{32}, adding to (23) and using the boundary conditions at S_{32} yields

$$\tfrac{1}{2}(1+\lambda_{32})\boldsymbol{u}_3(\boldsymbol{x}_s) = -\frac{\Omega}{\mathbb{C}_0\lambda_{21}}\int_{S_{32}} \boldsymbol{J}\cdot\boldsymbol{n}_3(\nabla_s\cdot\boldsymbol{n}_3)\,\mathrm{d}S - (1-\lambda_{32})\int_{S_{32}} \boldsymbol{u}_3\cdot\boldsymbol{K}\cdot\boldsymbol{n}_3\,\mathrm{d}S + \int_{S_{21}} \boldsymbol{J}\cdot\boldsymbol{T}_2\cdot\boldsymbol{n}_2\,\mathrm{d}S + \int_{S_{21}} \boldsymbol{u}_1\cdot\boldsymbol{K}\cdot\boldsymbol{n}_2\,\mathrm{d}S. \tag{25}$$

Equations (20), (22), (24) and (25) represent four integral equations for the four unknowns, $\boldsymbol{u}_1$ and $\boldsymbol{T}_2\cdot\boldsymbol{n}_2$ for $\boldsymbol{x}_s \in S_{21}$ and $\boldsymbol{u}_3$ and $\boldsymbol{T}_2\cdot\boldsymbol{n}_2$ for $\boldsymbol{x}_s \in S_{32}$. If $\boldsymbol{u}_\infty$, $\mathbb{C}_0$, the fluid

properties ($\lambda_{21}, \lambda_{32}$ and Ω) and the shapes of the fluid–fluid interfaces are specified, then these equations can be used to solve uniquely for the interfacial velocities. The evolution of the interfaces is followed using the kinematic conditions (6) and, consequently, the globule shape is determined for all times by an initial condition and the time history of the flow (Rallison 1984).

This system of equations is coupled; for example, determination of $\boldsymbol{u}_1$ requires knowledge of $\boldsymbol{u}_3$ and vice versa. The basic numerical procedure for this problem is similar to the one used in our earlier time-dependent studies of drop relaxation and breakup (Stone & Leal 1989*a*). Rather than repeating the details here, the important aspects are summarized below.

We will consider concentric double emulsion drops and axisymmetric flows, where $\boldsymbol{u}_\infty$ is given by (3). In such cases, the azimuthal (θ) integration can be performed analytically and the surface integrals are reduced to line integrals. The resulting integral equations are solved by discretizing each of the interfaces into $2N$-2 elements with node points at the end of each element. The unknowns (both velocities and stresses) are assumed to vary linearly over each element. This representation yields smoother and more accurate interfacial velocity and stress distributions than the alternative assumption of constant velocity and stress values over each element. Typically, for the calculations presented in this paper, we choose $N = 15$–20. At each node point there are four unknowns: two components of velocity (u_r, u_z) and two components of stress ($(\boldsymbol{T}\cdot\boldsymbol{n})_r, (\boldsymbol{T}\cdot\boldsymbol{n})_z$). Owing to the fore–aft symmetry of the extensional flow, the net number of unknowns is halved so that the largest linear system generated is 160×160. This linear system of equations is solved by Gaussian elimination.

The drop shapes are represented accurately by parameterizing each interface using a normalized measure of arclength, s ($0 \leqslant s \leqslant 1$), and describing the location of the surface node points with the cylindrical coordinates $r(s)$ and $z(s)$. Cubic splines are used to generate twice-continuously differentiable representations of the drop shape. The unit normals and curvature ($\nabla_s\cdot\boldsymbol{n}$) are calculated from the cubic spline representation.

After the interfacial velocities are calculated, the kinematic condition is used to update the interface shape. A simple Euler method is used for this purpose. Velocities are typically $O(10^{-3})$ so that the timestep chosen is typically $\Delta t = 0.3$–0.5. After each iteration, the collocation points are redistributed evenly, based upon arclength, along the interface. This minimizes convection of points that leads to uneven node point distributions and is a principal cause of numerical difficulties. A typical simulation to determine the deformation parameter D as a function of capillary number requires approximately 5000 iterations to map the entire steady deformation curve. Choosing $N = 20$, one iteration takes about one minute of CPU time on a SUN 3/160 workstation with a floating-point accelerator and using additional node points yields the same results. The steady shapes are calculated by requiring the normal velocities on both interfaces to be typically less than 2×10^{-4}–3×10^{-4} at each node point. In our previous numerical studies of drop deformation, concentrating the boundary elements in regions of large curvature improved the accuracy and, indeed, was necessary for following dynamics of drop breakup. However, no such implementation is introduced for the drop shapes typical of this study.

The numerical algorithm has been checked against the analytical results of Barthès-Biesel & Acrivos (1973*a*) for the deformation of single-phase droplets in axisymmetric extensional flows (this comparison is reported in Stone & Leal 1989*a*). The agreement is excellent. Comparison with the small deformation analysis

presented in §4 is shown in the results section that follows. The volumes of both the inner and outer droplets are monitored as time progresses and for $\lambda_{21} = O(1)$ and $\lambda_{32} = O(1)$ are found to change by less than 1% over several thousand iterations. As other researchers have found, larger volume changes occur for smaller λ, say $\lambda \approx 0.1$ or smaller.

6. Numerical study of finite deformation: results

In this section we summarize our numerical observations of the deformation and breakup of double emulsion droplets in axisymmetric extensional flows. Both steady-state and time-dependent effects are discussed.

We begin our discussion with a short comparison of the numerical results with the small deformation analysis from §4. In figure 9 the differences between the numerically predicted deformations of the inner and outer surfaces and the analytically calculated deformations ($D_{\text{numer}} - D_{\text{theory}}$) are plotted as a function of capillary number for a uniaxial extensional flow and several different combinations of $\lambda_{21}, \lambda_{32}, \kappa$ and Ω. Beginning with a spherical initial shape, the capillary number is increased in small increments (typically $\Delta\mathbb{C}_0 = 0.005$), the steady shape is calculated and then the capillary number is incremented again. As discussed in §4, a double emulsion globule placed in a uniaxial extensional flow will deform into a prolate ellipsoidal shape ($D > 0$) and at steady state the inner droplet will deform into an oblate ellipsoidal shape ($D < 0$). In figure 9 the basic trend is good agreement between the numerical results and the analytical theory for sufficiently small capillary numbers. However, as the capillary number is increased, the analytical theory consistently underpredicts the numerical values of D for the outer shape and overpredicts the deformation of the inner surface. The level of agreement shown in figure 9 is comparable to that found earlier for single-phase drops. Although it gives insight, the small deformation analysis of §4 is quantitatively limited even for relatively small values of $\mathbb{C}$ and for the remainder of this paper we will use numerical simulations to focus on the effects of finite deformation.

Steady state shapes characteristic of the early stages of deformation were shown in figures 3 and 4, so we next consider the time-dependent response of these multiphase droplets to step changes in shear rate for a uniaxial extensional flow. Figure 10 shows plots of the deformation of the inner and outer interfaces as a function of time for the case of a step change in shear rate from $\mathbb{C}_0 = 0.04 \rightarrow \mathbb{C}_0 = 0.08$. The other parameters are $\lambda_{21} = \lambda_{32} = 1.0, \Omega = 1.0$ and $\kappa = 0.5$.

The initial response of the globule to the step change in shear rate is to lengthen along the z-direction. This stretching process sets up a transient uniaxial stretching flow internal to the globule that results initially in a corresponding stretching of the inner droplet. Because the inner droplet has been deformed into an oblate spheroidal shape owing to the biaxial character of the initial steady flow in the annular region, the effect of this transient stretching process is to decrease the degree of deformation of the inner droplet. In other words, the inner droplet begins with a steady oblate shape and responds to the step change by deforming towards a spherical shape. However, as the new steady globule shape is approached, the flow in the annular region becomes a recirculating vortical motion and the inner droplet once again begins to stretch into an oblate spheroidal shape owing to the biaxial character of the flow (figures 2 and 3). Overall, the outer interface monotonically approaches the new steady shape, while the inner droplet relaxes initially then rapidly deforms back toward an oblate shape, until it finally asymptotically approaches a new steady

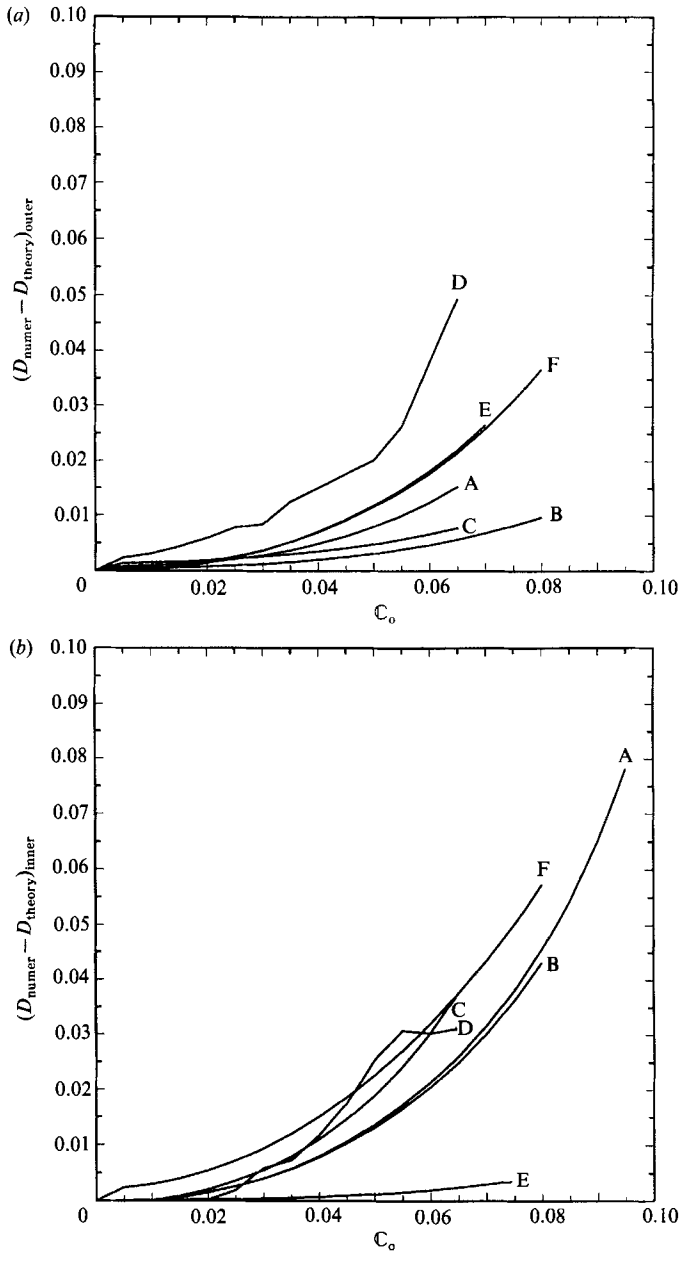

FIGURE 9. A comparison of numerical and theoretical predictions for globule deformation and wide range of parameter values. (*a*) D_{outer} *vs.* $\mathbb{C}_o$ (*b*) D_{inner} *vs.* $\mathbb{C}_o$. Typically agreement is good at low capillary numbers, but worsens as the capillary number, and hence the deformation, increases.

Curve	κ	λ_{21}	λ_{32}	Ω
A	0.5	10.0	1.0	1.0
B	0.5	1.0	1.0	1.0
C	0.5	1.0	10.0	1.0
D	0.8	1.0	1.0	1.0
E	0.3	1.0	1.0	1.0
F	0.2	1.0	1.0	0.1

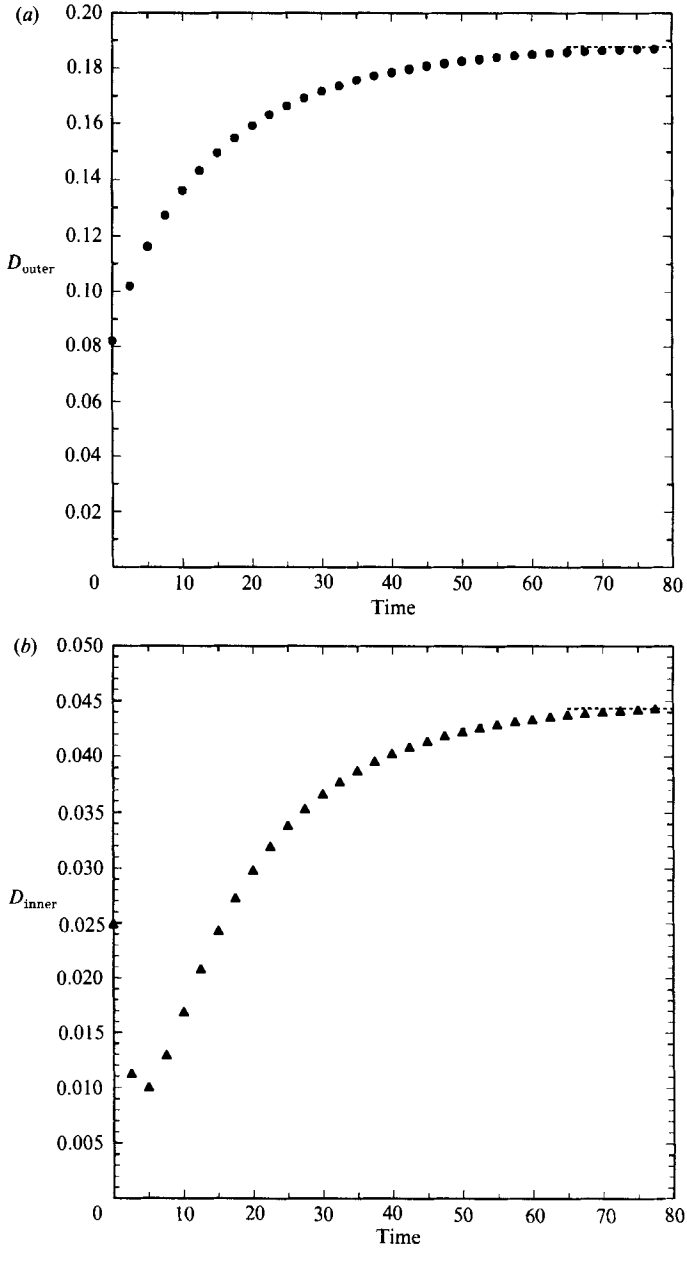

FIGURE 10. Time-dependent response of the globule deformation to a step change in shear rate, $\mathbb{C}_0 = 0.04 \rightarrow \mathbb{C}_0 = 0.08$. (*a*) D_{outer} *vs.* time (*b*) D_{inner} *vs.* time. The dashed horizontal line indicates the steady state established by approaching $\mathbb{C}_0 = 0.08$ using small increments in the capillary number. $\lambda_{21} = 1.0, \lambda_{32} = 1.0, \Omega = 1.0, \kappa = 0.5$.

shape. The horizontal dashed lines in figure 10 denote the steady shapes observed at $\mathbb{C}_0 = 0.08$ by beginning with a spherical initial shape and making small increments in the capillary number ($\Delta\mathbb{C}_0 = 0.005$). Clearly, the same steady shape is determined using either large or small increments in the capillary number. The behaviour described above is typical of transient deformation below the critical capillary number.

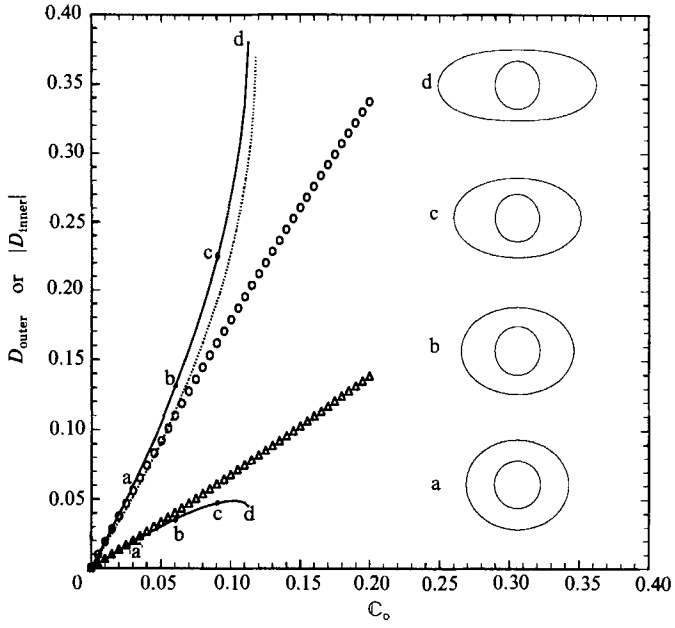

FIGURE 11. Complete numerical simulation of deformation as a function of the capillary number in a uniaxial extensional flow. $\lambda_{21} = \lambda_{32} = 1.0, \Omega = 1.0, \kappa = 0.5$. Several numerically generated steady shapes are included. The upper solid line represents D_{outer} *vs.* $\mathbb{C}_o$, the lower solid line represents $|D_{inner}|$ *vs.* $\mathbb{C}_o$ and the symbols are predictions of the small deformation theory. The dashed curve represents the deformation of a single-phase droplet of comparable viscosity. The curves are stopped when breakup is indicated by continuous stretching of the droplet.

We next address finite deformation and breakup of compound drops. In figure 11 the solid curve shows a complete numerical simulation of the steady-state globule deformation as a function of capillary number for a uniaxial extensional flow ($\lambda_{21} = \lambda_{32} = 1.0, \Omega = 1.0$ and $\kappa = 0.5$). The dashed curve is the equivalent single-phase droplet deformation and the lower solid curve is the absolute value of the deformation of the inner droplet. Numerically generated shapes are also shown. The numerical simulation is stopped when a steady shape can no longer be achieved and the globule begins to stretch continuously. The symbols are the theoretical results from §4.

As mentioned above, the small deformation theory provides a good approximation to the actual deformation at small capillary numbers. In this range, the deformation of the globule is larger with the occluded droplet present than without it present. It can be seen in figure 11 that this increase of deformation is maintained over the whole range of capillary numbers up to the critical value, $\mathbb{C}_o \approx 0.116$. At this point, the globule begins to undergo a continuous stretching process so that breakup is characterized in this case by the non-existence of a steady shape. The numerical results indicate that the critical capillary number for breakup is slightly lower with the inner droplet present than without it. This was first suggested on the basis of small deformation theory by Davis & Brenner (1981) and also by the analysis of §4. However, it should be clear that the linear theory presented in §§3–4 is no longer valid near the critical capillary number where finite deformation has occurred. Also, the numerical calculations indicate that the globule has a slightly more extended final steady shape than the corresponding single-phase drop. However, the difference

relative to the single-phase drop is small and because the determination of the steady shape is difficult as the critical capillary number is approached, the result mainly indicates that the overall globule shape changes relatively little owing to the presence of the occluded particle. Nevertheless, it is easier to break. In this simulation the critical capillary number necessary for breakup is reduced by approximately 5% from the single-phase drop result.

Finally, we mention the behaviour of the inner droplet. The steady-state velocity field in the annular region will be biaxial in nature. The deformation of the inner droplet increases monotonically until its deformation levels off and then even decreases slightly near the critical capillary number. Overall, however, there is very little distortion of the inner drop, in part because the inner capillary number is smaller than the outer capillary number ($\mathbb{C}_i = 0.5\mathbb{C}_o$). Nevertheless, the levelling off of the deformation is due to a combination of hydrodynamic interaction between the finitely deformed fluid–fluid interfaces and the consequent effect the deformed interface shapes have on the velocity field internal to the globule. These observations suggest that the relevant effective capillary number for the inner drop is more appropriately of the form $\mathbb{C}_{i\,\mathrm{eff}} = \beta G R_2 \mu_2/\sigma_{32}$, where β represents the decrease of the internal velocity gradient from $O(G)$ to $O(\beta G)$, $\beta < 1$. Although useful conceptually, this idea has not provided additional quantitative predictions.

In order to examine the dynamics of breakup, figure 12 presents the dimensionless globule length, L_{outer}/R_1, as a function of time at the critical capillary number (the solid curve). The evolution of the dimensionless inner droplet length, L_{inner}/R_2, is also plotted in this figure (the dashed curve), along with numerically generated shapes. The slow initial extension and the extended character of the globule are similar to observations of single-phase droplets at the critical capillary number. The midsection becomes cylindrical and as the globule becomes more extended it stretches more rapidly. As the globule stretches, the flow field internal to the globule is extensional also, so that the inner droplet begins to lengthen slightly and deforms into a prolate spheroidal shape, although the overall inner deformation is much smaller in this case than for the globule. However, the thinning of the globule occurs more rapidly than the inner droplet can deform and the result is the formation of a very thin film between the two interfaces. Shortly after the final shape illustrated, the numerical scheme begins to introduce unrealistic oscillations on the inner surface. Additional collocation points are necessary to describe accurately the variations in interfacial velocity and stress that occur for these elongated globules with thin films between the surfaces. However, the formation of a thin-film configuration for this particular set of dimensionless parameters suggests the possibility of breakup of the extended globule owing to fracture at the middle induced by the presence of the inner droplet. This mode of breakup clearly has no counterpart in the case of a single-phase drop, which previous studies have shown to stretch continuously to a very thin thread in the presence of a steady, uniaxial extensional flow at the critical capillary number. Another possibility suggested by this simulation is that the inner droplet would also stretch sufficiently so that, at later times, the globule would begin to approach a configuration similar to a concentric multiphase fluid cylinder. However, at least for the case considered in figure 12, it appears that breakup due to pinching about the occluded particle occurs instead.

In figure 13 we present another complete simulation of the steady-state deformation curve for a double emulsion drop in the case $\lambda_{21} = 1.0, \lambda_{32} = 10.0, \Omega = 1.0$ and $\kappa = 0.5$ (so $\mathbb{C}_i = 0.5\mathbb{C}_o$). Here we specifically examine the effect of a large viscosity of the occluded particle. The two solid curves represent the deformation of

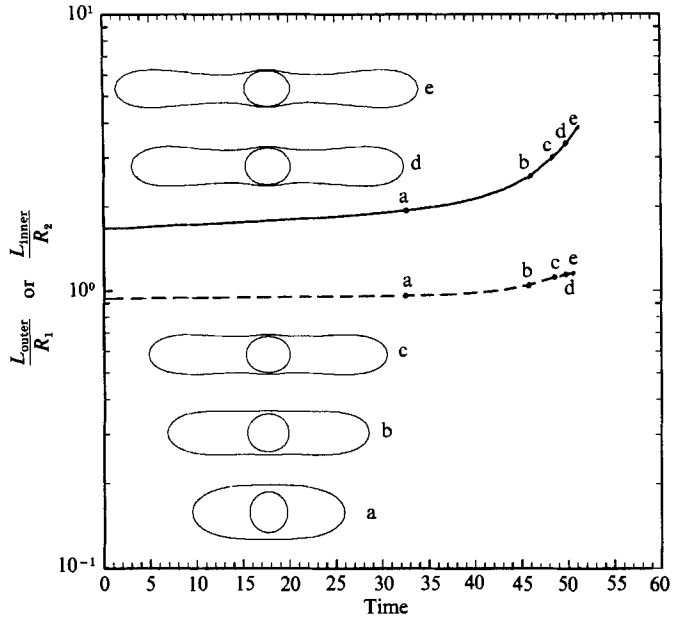

FIGURE 12. Globule length versus time for elongation at a slightly supercritical capillary number. The solid curve is the globule length L_{outer}/R_1 and the dashed curve is the length of the inner droplet L_{inner}/R_2.

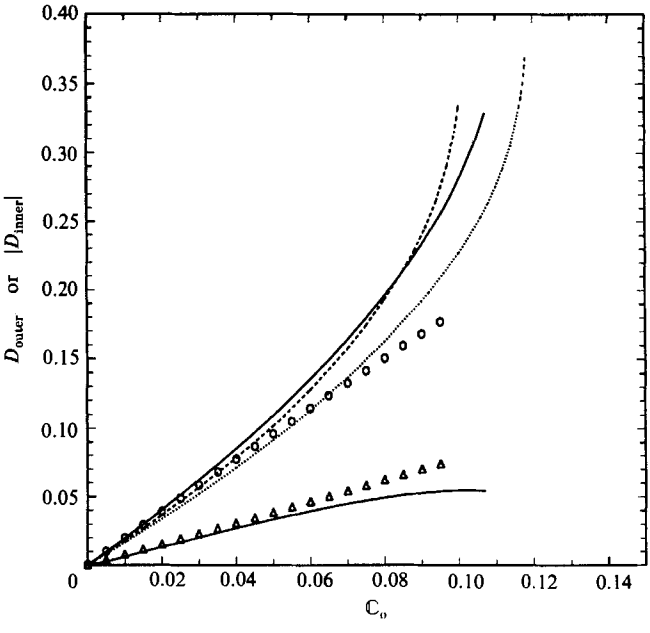

FIGURE 13. Double emulsion deformation as a function of capillary number for a viscous occluded particle. $\lambda_{21} = 1.0, \lambda_{32} = 10.0, \kappa = 0.5$ and $\Omega = 1.0$. The solid curves are the outer and inner droplet deformations respectively. The short dashed line is a single-phase droplet with $\lambda = 1.0$ and the long dashed line is a single-phase droplet with $\lambda = 10.0$.

the outer and inner surfaces. The short dashed line is the deformation of a single-phase drop with $\lambda = 1.0$ and the long dashed line is the deformation of a single-phase drop with $\lambda = 10.0$ (for single-phase drops λ represents the ratio of drop viscosity to suspending fluid viscosity). We observe that the critical capillary number for breakup of the globule is bounded by the single-phase results. The inner drop deforms monotonically until the critical capillary number is approached at which point the deformation levels off and decreases a little. This is similar to the deformation shown in figure 11. We also see that the single-phase drop with $\lambda = 10.0$ is initially less deformed than the double emulsion drop, but as the capillary number is increased the single-phase drop deforms more and breaks at a lower capillary number.

The effect on globule deformation of varying λ_{32} is illustrated clearly in figure 14. Although the magnitude of the final steady-state distortions differ by a small amount, it is noteworthy that the globule (D_{outer}) is always more deformed for larger viscosities of the internal droplet, as suggested by the small deformation analysis. Also, it is evident that as the viscosity of the inner droplet is increased the critical capillary number needed for breakup of the globule decreases slightly. In all of the cases considered in figure 14, breakup occurs via the continuous stretching process that is characteristic of the non-existence of a steady shape, as shown in figure 12. Although the critical capillary number does not change much relative to the single-phase drop, it is important to keep in mind the fundamental change which occurs in the mode of breakup. For example, the degree of extension necessary to produce breakup with the occluded drop present is generally going to be much lower than that necessary for a single-phase drop, and this could have important implications in the design of emulsifiers or flow systems to transport multiphase drops.

In figure 15 we examine the deformation and breakup of a globule containing a large internal droplet. For this simulation we choose $\kappa = 0.8, \lambda_{21} = 1.0, \lambda_{32} = 1.0$ and $\Omega = 1.0$ ($\mathbb{C}_i = 0.8\mathbb{C}_o$). On the plot of deformation versus capillary number, numerically generated globule shapes are included to illustrate the interfacial evolution. As in previous figures the effect of the uniaxial extensional flow is to deform the outer surface into a prolate spheroidal shape while the inner surface becomes oblate spheroidal. However, in this case, at a capillary number $\mathbb{C}_o = 0.066$ the two interfaces numerically make contact at the globule centre. The calculations are stopped at this point. Physically, the numerical contact of the two interfaces suggests breakup of the globule as a consequence of the inner droplet breaking through the outer surface. The breakup of the globule occurs in this case without any large-scale stretching and at a critical capillary number that is much lower than would be found for a single-phase drop with the same properties as the suspending fluid. Furthermore, unlike previous cases where 'breakup' has been identified with the non-existence of steady solutions, leading to time-dependent stretching of the globule and only eventually to breakup via instability of the thin thread, 'breakup' here would presumably occur rapidly without further extension of the drop owing to breakdown of the thin film. In other words, incompatibility of the steady inner and outer interface shapes leads to globule burst, even though the globule is only modestly deformed. Although the numerical simulations cannot capture the actual breakup process since intermolecular forces that become important at small separations are not included, this example demonstrates a second mechanism of globule breakup that may be important for large κ.

The effect of κ on globule deformation and the critical capillary number for breakup is illustrated in figure 16. Clearly, the conjecture, based on the small deformation

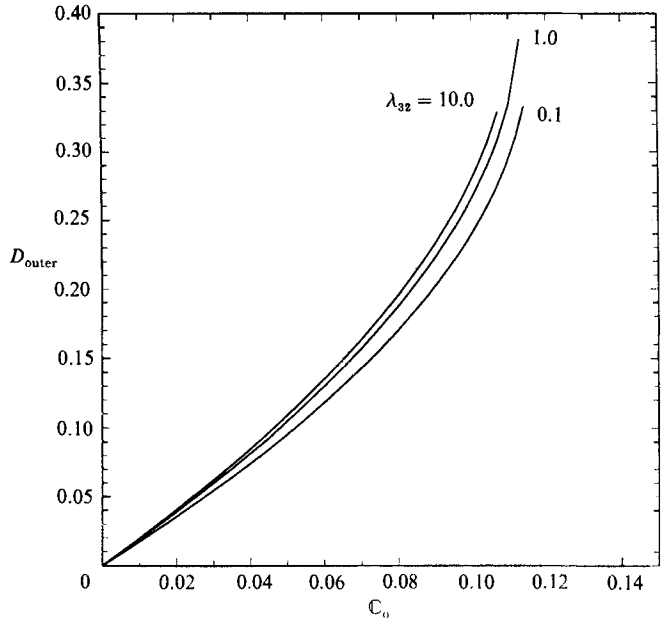

FIGURE 14. The effect of λ_{32} on drop deformation and the critical capillary number for breakup. $\lambda_{21} = 1.0, \Omega = 1.0$ and $\kappa = 0.5$.

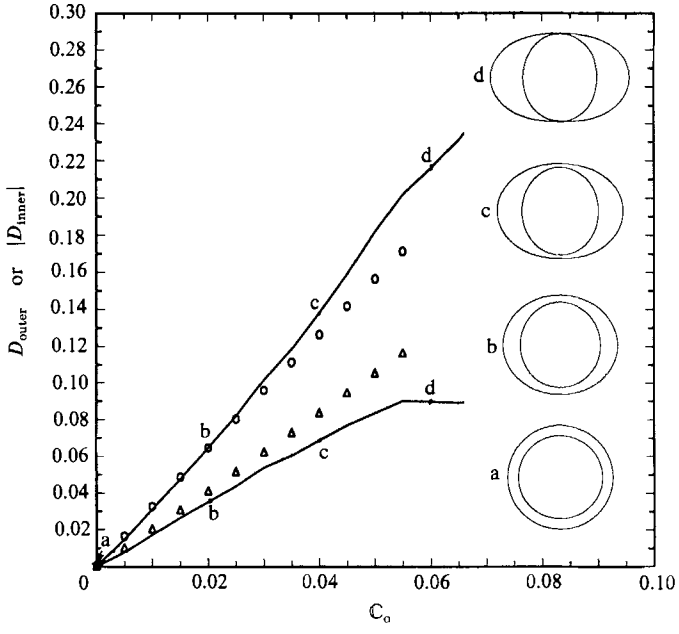

FIGURE 15. Deformation as a function of capillary number for a large internal droplet. $\lambda_{21} = \lambda_{32} = 1.0, \Omega = 1.0$ and $\kappa = 0.8$.

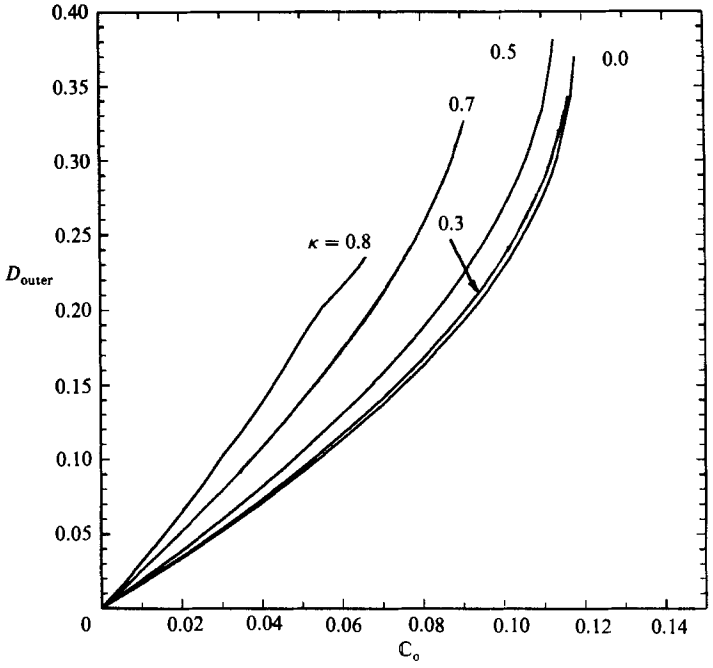

FIGURE 16. The effect of κ on the deformation as a function of capillary number and effect on the critical capillary number necessary for breakup. The low capillary number for breakup at $\kappa = 0.8$ is a consequence of the inner drop making contact with the outer surface. In the $\kappa = 0.7$ simulation, a narrow film is formed between the inner and outer interfaces simultaneously with large globule deformation and it is not clear which of the two breakup mechanisms described in the text occurs first.

analysis, that the presence of the occluded particle leads to lower capillary numbers for breakup, is true. However, as illustrated in figure 15, the very low critical capillary number for breakup at $\kappa = 0.8$ is not a consequence of large deformation of the globule, but rather occurs owing to the inner drop making contact with the outer surface. Meanwhile, in the $\kappa = 0.7$ simulation, a very narrow film is formed between the two interfaces simultaneously with large globule deformation and it is not clear which of the two breakup mechanisms occurs first.

Finally, as an illustration of effects of flow-type and large internal capillary numbers, $\mathbb{C}_i$, we consider the case of a globule suspended in a biaxial extensional flow. Figure 17 shows the deformation plotted versus capillary number and includes intermediate steady shapes typical of the deformation process. The parameters chosen are $\lambda_{21} = \lambda_{32} = 1.0, \kappa = 0.5$ and $\Omega = 0.1$ ($\mathbb{C}_i = 5\mathbb{C}_o$). The biaxial flow deforms the globule into an oblate spheroidal shape and the steady uniaxial flow established in the annular region deforms the inner drop into a prolate spheroidal shape. Because lower capillary numbers are needed for breakup of a drop in uniaxial extensional flows, we have purposely chosen a low value of Ω. Clearly, the outer droplet deforms very little. However, viscous stresses generated internal to the globule stretch the occluded droplet into a rather extended prolate spheroid. The low value of Ω (hence a larger internal effective capillary number $\mathbb{C}_i = 5\mathbb{C}_o$), coupled with the uniaxial nature of the flow field in the annular region produces a large distortion of the inner droplet. Indeed, the deformation of the inner droplet is approaching the most highly deformed steady shape observed for a single-phase drop suspended in an unbounded

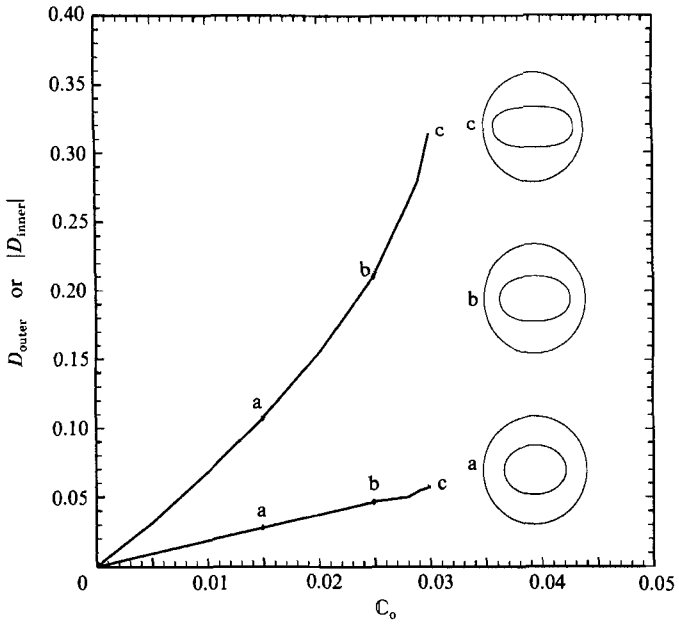

FIGURE 17. Deformation of a double emulsion droplet in a biaxial extensional flow. $\lambda_{21} = \lambda_{32} = 1.0, \kappa = 0.5$ and $\Omega = 0.1$.

uniaxial extensional flow. This suggests that the inner drop may undergo breakup even though the outer drop is itself not very deformed. Shortly after the final steady shape shown the numerical scheme begins to break down and additional collocation points and a smaller timestep are necessary to continue the calculations further. Nevertheless, this example illustrates that, in some instances, the effect of flow-type coupled with the flow-induced deformation internal to the double emulsion droplet can produce large distortions and possibly internal breakup.

7. Conclusions

The analytic and numerical results presented above describe the deformation and possible breakup mechanisms of double emulsion droplets in extensional flows. The simulations provide insight as to when analogies with single-phase droplet behaviour may be useful. With the exception of figure 17, the numerical calculations have been limited to the case when the internal capillary number is small. Nevertheless, two distinct mechanisms of globule breakup have been suggested, both having in common the feature that the inner drop appears as an 'obstacle' for the outer interface. The effect of large internal capillary numbers has not been systematically studied.

From this work, the following conclusions and observations can be drawn:

(i) A uniaxial extensional flow deforms the globule into a prolate spheroidal shape while the steady recirculating flow generated in the annular region deforms the occluded drop into an oblate spheroidal shape. The reverse holds for a globule placed in a biaxial extensional flow.

(ii) The effective viscosity of a dilute emulsion of compound drops behaves like a suspension of solid spheres in the limit of almost equal-sized inner and encapsulating drops, $\kappa \to 1$.

(iii) The presence of the internal droplet produces breakup at a lower value of the capillary number than is necessary if no third phase is present. Also, as the viscosity of the occluded phase is increased, the critical capillary number for breakup decreases.

(iv) Although a complete study of variations in viscosity ratio has not been undertaken, the simulations with $\lambda_{21} = O(1)$ and $\lambda_{32} = O(1)$ suggest that for $\kappa < 0.5$ breakup of the globule occurs by a continuous stretching mode. However, for $\kappa \approx 0.8$ the inner and outer interfaces make contact even though the globule is not very deformed (incompatibility of steady interface shapes).

(v) The application of a biaxial flow produces a uniaxial flow internal to the globule that is capable of producing large distortions of the occluded drop. For a low value of the interfacial tension of the inner drop ($\Omega = 0.1$), a simulation is illustrated suggesting breakup of the inner phase even though the outer drop is not very deformed.

This work was supported by a grant to L. G. L. from the fluid mechanics program of the National Science Foundation. H. A. S. was partially supported through an IBM Graduate Research Fellowship.

Appendix A

In this Appendix we present some of the details of the solution for the velocity fields interior and exterior to the double emulsion drop. The basic equations and boundary conditions are given in §3.

At steady state the kinematic condition (6) at S_{21} is $\boldsymbol{n}_2^\circ \cdot \boldsymbol{u}_1 = \boldsymbol{n}_2^\circ \cdot \boldsymbol{u}_2 = 0$ for $\boldsymbol{x}_s = \boldsymbol{n}_2^\circ, r = 1$, which yields

$$1 + \tfrac{1}{2}B_1 - 3C_1 = 2F_2 + \tfrac{1}{2}B_2 - 3C_2 + \tfrac{3}{21}H_2 = 0,$$

and continuity of the tangential velocity at S_{21} requires

$$1 + 2C_1 = 2F_2 + 2C_2 + \tfrac{5}{21}H_2,$$

$$\tfrac{1}{2} + D_1 = G_2 + D_2.$$

The kinematic and continuity of velocity conditions at S_{32} yield the relationships

$$2\kappa F_2 + \frac{1}{2\kappa^2}B_2 - \frac{3}{\kappa^4}C_2 + \frac{3\kappa^3}{21}H_2 = 2\kappa F_3 + \frac{3\kappa^3}{21}H_3 = 0,$$

$$2\kappa F_2 + \frac{2}{\kappa^4}C_2 + \frac{5\kappa^3}{21}H_2 = 2\kappa F_3 + \frac{5\kappa^3}{21}H_3,$$

$$\kappa G_2 + \frac{1}{\kappa^2}D_2 = \kappa G_3.$$

Finally, the tangential stress balance at the two interfaces provides the four equations

$$2 + B_1 - 16C_1 = \lambda_{21}(4F_2 + B_2 - 16C_2 + \tfrac{16}{21}H_2), \quad D_1 = \lambda_{21}D_2,$$

$$4F_2 + \frac{1}{\kappa^3}B_2 - \frac{16}{\kappa^5}C_2 + \frac{16\kappa^3}{21}H_2 = \lambda_{32}\left(4F_3 + \frac{16\kappa^2}{21}H_3\right), \quad D_2 = 0.$$

It is immediately evident at this point that

$$D_1 = 0, \quad D_2 = 0, \quad G_2 = \tfrac{1}{2} = G_3.$$

The complete solution of the remaining 8 equations for the 8 remaining unknowns requires tedious algebra. The results are:

$$B_1 = \frac{3\left[(4-25\kappa^3+42\kappa^5-25\kappa^7+4\kappa^{10})+\dfrac{\kappa^3}{1+\lambda_{32}}(15-42\kappa^2+35\kappa^4-8\kappa^7)\right]}{\eta_1+\dfrac{\kappa^3}{1+\lambda_{32}}\eta_2}-5,$$

$$B_2 = \frac{3\left[\kappa^3(10-14\kappa^2+4\kappa^7)+\dfrac{\kappa^3}{1+\lambda_{32}}2(-3+7\kappa^2-4\kappa^7)\right]}{\eta_1+\dfrac{\kappa^3}{1+\lambda_{32}}\eta_2},$$

$$C_1 = \frac{\frac{1}{2}\left[(4-25\kappa^3+42\kappa^5-25\kappa^7+4\kappa^{10})+\dfrac{\kappa^3}{1+\lambda_{32}}(15-42\kappa^2+35\kappa^4-8\kappa^7)\right]}{\eta_1+\dfrac{\kappa^3}{1+\lambda_{32}}\eta_2}-\tfrac{1}{2},$$

$$C_2 = \frac{\kappa^5(3-5\kappa^2+2\kappa^5)+\dfrac{\kappa^3}{1+\lambda_{32}}\kappa^2(-3+7\kappa^2-4\kappa^5)}{\eta_1+\dfrac{\kappa^3}{1+\lambda_{32}}\eta_2},$$

$$F_2 = -\frac{\frac{3}{2}\left[(2-7\kappa^5+5\kappa^7)+\dfrac{\kappa^3}{1+\lambda_{32}}7\kappa^2(1-\kappa^2)\right]}{\eta_1+\dfrac{\kappa^3}{1+\lambda_{32}}\eta_2},$$

$$F_3 = -\frac{\dfrac{3}{2(1+\lambda_{32})}(-3+7\kappa^2-7\kappa^5+3\kappa^7)}{\eta_1+\dfrac{\kappa^3}{1+\lambda_{32}}\eta_2},$$

$$H_2 = \frac{21\left[(2-5\kappa^3+3\kappa^5)+\dfrac{\kappa^3}{1+\lambda_{32}}3(1-\kappa^2)\right]}{\eta_1+\dfrac{\kappa^3}{1+\lambda_{32}}\eta_2},$$

$$H_3 = \frac{\dfrac{21}{\kappa^2(1+\lambda_{32})}(-3+7\kappa^2-7\kappa^5+3\kappa^7)}{\eta_1+\dfrac{\kappa^3}{1+\lambda_{32}}\eta_2},$$

where $\eta_1 = (4-25\kappa^3+42\kappa^5-25\kappa^7+4\kappa^{10})+\lambda_{21}(4-10\kappa^3+10\kappa^7-4\kappa^{10})$,

$\eta_2 = (15-42\kappa^2+35\kappa^4-8\kappa^7)+\lambda_{21}(6-14\kappa^4+8\kappa^7)$.

The steady-state velocity field thus calculated is a uniformly valid first approximation to the flow field for all values of κ, λ_{21} and λ_{32}, provided the interface deformation is small. However, as is clear from the related analysis of the single-

phase droplet deformation problem, this velocity field is not sufficient to calculate the first correction to the drop shapes for very viscous droplets, either $\lambda_{21} \gg 1$ or $\lambda_{32} \gg 1$. This is because the next term in an asymptotic expansion for the velocity field makes an order-one contribution in the normal stress balance if the viscosity ratio is large (Barthes-Biesel & Acrivos 1973*a*; Rallison 1980; Davis & Brenner 1981). We have not calculated this correction and have relegated the effect of large viscosity ratios to the numerical investigation that is reported in §§5–6.

If we consider the case where $\lambda_{21} = O(1)$ and $\lambda_{32} = O(1)$, then for $\mathbb{C} \ll 1$ the velocity field just determined can be used in the normal stress balance to calculate the first correction to the drop shape. Equations (5*d*, *e*) and (11*a*, *b*) relate the constant pressures by

$$p_2^\circ = \frac{2}{\mathbb{C}_o} + p_\infty,$$

$$p_3^\circ = \left(2 + \frac{2}{\kappa}\right)\frac{1}{\mathbb{C}_o} + p_\infty,$$

and provide the two additional equations that are necessary to determine the shape correction functions A_{21} and A_{32} at this leading order of approximation,

$$1 - 3B_1 + 24C_1 - \lambda_{21}(F_2 - 3B_2 + 24C_2 - \tfrac{3}{21}H_2) = \frac{4}{\mathbb{C}_o A_{21}},$$

$$4F_2 - \frac{3}{\kappa^3}B_2 + \frac{24}{\kappa^5}C_2 - \frac{3\kappa^2}{21}H_2 - \lambda_{32}\left(4F_3 - \frac{3\kappa^2}{21}H_3\right) = \frac{4\Omega}{\mathbb{C}_o \lambda_{21}\kappa}A_{32} = \frac{4}{\mathbb{C}_i}A_{32}.$$

Using these equations the shape correction functions A_{21} and A_{32} may be expressed in the form

$$A_{21} = \tfrac{1}{4}\mathbb{C}_o h_{21}(\kappa, \lambda_{21}, \lambda_{32}),$$

$$A_{32} = \tfrac{1}{4}\mathbb{C}_i h_{32}(\kappa, \lambda_{21}, \lambda_{32}),$$

where

$$\begin{aligned} h_{21} = {} & 5 + [-(6 + 4\lambda_{21}) + (30\kappa^3 - 24\kappa^5)(1 - \lambda_{21})]F_2 \\ & + [(-3 + 63\kappa^5 - 60\kappa^7)(1 - \lambda_{21})]H_2 + (-30\kappa^3 + 24\kappa^5)(1 - \lambda_{21})F_3 \\ & + (-63\kappa^5 + 60\kappa^7)(1 - \lambda_{21})H_3, \end{aligned}$$

and

$$h_{32} = 10F_2 - (6 + 4\lambda_{32})F_3 - 3\kappa^2(1 - \lambda_{32})H_3.$$

Appendix B

In this Appendix we report the form of the stress fields corresponding to the velocity and pressure fields reported in §3. They are:

$$\begin{aligned} \boldsymbol{T}_1(\boldsymbol{x}) = {} & 2\boldsymbol{E} + B_1\left[\frac{(\boldsymbol{E}\cdot\boldsymbol{x})\boldsymbol{x} + \boldsymbol{x}(\boldsymbol{E}\cdot\boldsymbol{x})}{r^5} - 5\frac{\boldsymbol{x}\boldsymbol{x}(\boldsymbol{x}\cdot\boldsymbol{E}\cdot\boldsymbol{x})}{r^7}\right] + C_1\left[-20\frac{(\boldsymbol{E}\cdot\boldsymbol{x})\boldsymbol{x}}{r^7}\right. \\ & \left. - 20\frac{\boldsymbol{x}(\boldsymbol{E}\cdot\boldsymbol{x})}{r^7} - 10\frac{\boldsymbol{I}(\boldsymbol{x}\cdot\boldsymbol{E}\cdot\boldsymbol{x})}{r^7} + 70\frac{\boldsymbol{x}\boldsymbol{x}(\boldsymbol{x}\cdot\boldsymbol{E}\cdot\boldsymbol{x})}{r^9} + 4\frac{\boldsymbol{E}}{r^5}\right] \\ & - 3D_1\left[\frac{\boldsymbol{x}(\boldsymbol{\omega}\wedge\boldsymbol{x}) + (\boldsymbol{\omega}\wedge\boldsymbol{x})\boldsymbol{x}}{r^5}\right], \end{aligned}$$

$$\boldsymbol{T}_2(\boldsymbol{x}) = 4F_2\boldsymbol{E} + B_2\left[\frac{(\boldsymbol{E}\cdot\boldsymbol{x})\boldsymbol{x} + \boldsymbol{x}(\boldsymbol{E}\cdot\boldsymbol{x})}{r^5} - 5\frac{\boldsymbol{x}\boldsymbol{x}(\boldsymbol{x}\cdot\boldsymbol{E}\cdot\boldsymbol{x})}{r^7}\right] + C_2\left[-20\frac{(\boldsymbol{E}\cdot\boldsymbol{x})\boldsymbol{x}}{r^7}\right.$$
$$\left. - 20\frac{\boldsymbol{x}(\boldsymbol{E}\cdot\boldsymbol{x})}{r^7} - 10\frac{\boldsymbol{I}(\boldsymbol{x}\cdot\boldsymbol{E}\cdot\boldsymbol{x})}{r^7} + 70\frac{\boldsymbol{x}\boldsymbol{x}(\boldsymbol{x}\cdot\boldsymbol{E}\cdot\boldsymbol{x})}{r^9} + 4\frac{\boldsymbol{E}}{r^5}\right]$$
$$- 3D_2\left[\frac{\boldsymbol{x}(\boldsymbol{\omega}\wedge\boldsymbol{x}) + (\boldsymbol{\omega}\wedge\boldsymbol{x})\boldsymbol{x}}{r^5}\right] + H_2[\tfrac{6}{21}[\boldsymbol{x}(\boldsymbol{E}\cdot\boldsymbol{x}) + (\boldsymbol{E}\cdot\boldsymbol{x})\boldsymbol{x}]$$
$$+ \tfrac{10}{21}r^2\boldsymbol{E} - \tfrac{25}{21}\boldsymbol{I}(\boldsymbol{x}\cdot\boldsymbol{E}\cdot\boldsymbol{x})]$$
$$\boldsymbol{T}_3(\boldsymbol{x}) = 4F_3\boldsymbol{E} + H_3[\tfrac{6}{21}[\boldsymbol{x}(\boldsymbol{E}\cdot\boldsymbol{x}) + (\boldsymbol{E}\cdot\boldsymbol{x})\boldsymbol{x}] + \tfrac{10}{21}r^2\boldsymbol{E} - \tfrac{25}{21}\boldsymbol{I}(\boldsymbol{x}\cdot\boldsymbol{E}\cdot\boldsymbol{x})].$$

REFERENCES

ACRIVOS, A. 1983 The breakup of small drops and bubbles in shear flows. *4th Intl Conf. on Physicochemical Hydrodynamics. Ann. NY Acad. Sci* **404**, 1–11.

BARTHÈS-BIESEL, D. & ACRIVOS, A. 1973*a* Deformation and burst of a liquid droplet freely suspended in a linear shear field. *J. Fluid Mech.* **61**, 1–21.

BARTHÈS-BIESEL, D. & ACRIVOS, A. 1973*b* The rheology of suspensions and its relation to phenomenological theories for non-Newtonian fluids. *Intl J. Multiphase Flow* **1**, 1–24.

BATCHELOR, G. K. 1970 The stress system in a suspension of force-free particles. *J. Fluid Mech.* **41**, 545–570.

BENTLEY, B. J. & LEAL, L. G. 1986 An experimental investigation of drop deformation and breakup in steady two-dimensional linear flows. *J. Fluid Mech.* **167**, 241–283.

BRUNN, P. O. & RODEN, T. 1985 On the deformation and drag of a type-A multiple drop at low Reynolds number. *J. Fluid Mech.* **160**, 211–234.

CHERVENIVANOVA & ZAPRYANOV. 1988 On the deformation of compound multiphase drops at low Reynolds number. Submitted to *Intl J. Multiphase Flow.*

COX, R. G. 1969 The deformation of a drop in a general time-dependent fluid flow. *J. Fluid Mech.* **37**, 601–623.

DAVIS, A. M. J. & BRENNER, H. 1981 Emulsions containing a third solid internal phase. *J. Engng. Mech. Div. ASCE* **107**, 609–621.

FLORENCE, A. T. & WHITEHILL, D. 1981 Some features of breakdown in water-in-oil-in-water multiple emulsions. *J. Colloid Interface Sci.* **79**, 243–256.

FRANKEL, N. A. & ACRIVOS, A. 1970 The constitutive equation for a dilute emulsion. *J. Fluid Mech.* **44**, 65–78.

JOHNSON, R. E. 1981 Stokes flow past a sphere coated with a thin fluid film. *J. Fluid Mech.* **110**, 217–238.

JOHNSON, R. E. & SADHAL, S. S. 1983 Stokes flow past bubbles and drops partially coated with thin films. Part 2. Thin films with internal circulation – a perturbation solution. *J. Fluid Mech.* **132**, 295–318.

JOHNSON, R. E. & SADHAL, S. S. 1985 Fluid mechanics of compound multiphase drops and bubbles. *Ann. Rev. Fluid Mech.* **17**, 289–320.

LADYZHENSKAYA, O. 1969 *The Mathematical Theory of Viscous Incompressible Flow*, 2nd edn. Gordon & Breach.

LAMB, H. 1932 *Hydrodynamics*, 6th edn. Dover.

LEE, S. H. & LEAL, L. G. 1982 The motion of a sphere in the presence of a deformable interface. II. A numerical study of the translation of a sphere normal to an interface. *J. Colloid Interface Sci.* **87**, 81–106.

LI, N. N. 1971*a* Separation of hydrocarbons by liquid membrane permeation. *Ind. Engng. Chem. Process Des. Dev.* **10**, 215–221.

LI, N. N. 1971*b* Permeation through liquid surfactant membranes. *AIChE J.* **17**, 459–463.

MAUGH, T. H. 1976 Liquid membranes: New techniques for separation, purification. *Science* **193**, 134–137.

RALLISON, J. M. 1980 Note on the time-dependent deformation of a viscous drop which is almost spherical. *J. Fluid Mech.* **98**, 625–633.

RALLISON, J. M. 1981 A numerical study of the deformation and burst of a viscous drop in general shear flows. *J. Fluid Mech.* **109**, 465–482.

RALLISON, J. M. 1984 The deformation of small viscous drops and bubbles in shear flows. *Ann. Rev. Fluid Mech.* **16**, 45–66.

RALLISON, J. M. & ACRIVOS, A. 1978 A numerical study of the deformation and burst of a viscous drop in an extensional flow. *J. Fluid Mech.* **89**, 191–200.

RUSHTON, E. & DAVIES, G. A. 1983 Settling of encapsulated droplets at low Reynolds numbers. *Intl J. Multiphase Flow* **9**, 337–342.

SADHAL, S. S. & OGUZ, H. N. 1985 Stokes flow past compound multiphase drops: the case of completely engulfed drops/bubbles. *J. Fluid Mech.* **160**, 511–529.

SCHOWALTER, W. R., CHAFFEY, C. E. & BRENNER, H. 1968 Rheological behaviour of a dilute emulsion. *J. Colloid Interface Sci.* **26**, 152–160.

SHERWOOD, J. D. 1988 Breakup of fluid droplets in electric and magnetic fields. *J. Fluid Mech.* **188**, 133–146.

STONE, H. A. & LEAL, L. G. 1989*a* Relaxation and breakup of an initially extended drop in an otherwise quiescent fluid. *J. Fluid Mech.* **198**, 399–427.

STONE, H. A. & LEAL, L. G. 1989*b* A note concerning drop deformation and breakup in biaxial extensional flows at low Reynolds numbers. *J. Colloid Interface Sci.* (to appear).

STOOS, J. A. & LEAL, L. G. 1989 Particle motion in axisymmetric stagnation flow toward an interface *AIChE J.* **35**, 196–212.

STROEVE, P. & VARANASI, P. P. 1984 An experimental study on double emulsion drop breakup in uniform shear flow. *J. Colloid Interface Sci.* **99**, 360–373.

TAYLOR, G. I. 1932 The viscosity of a fluid containing small drops of another fluid. *Proc. R. Soc. Lond.* A **138**, 41–48.

TAYLOR, T. D. & ACRIVOS, A. 1964 On the deformation and drag of a falling viscous drop at low Reynolds number. *J. Fluid Mech.* **18**, 466–476.

TORZA, S. & MASON, S. G. 1969 Coalescence of two immiscible liquid drops. *Science* **163**, 813–814.

TORZA, S. & MASON, S. G. 1970 Three-phase interactions in shear and electrical fields. *J. Colloid Interface Sci.* **33**, 67–83.

TSAMOPOULOS, J. A. & BROWN, R. A. 1987 Dynamic centering of liquid shells. *Phys. Fluids* **30**, 27–35.

ULBRECHT, J. J., STROEVE, P. & PRABODH, P. 1982 Behaviour of double emulsions in shear flows. *Rheol. Acta* **21**, 593–597.

YOUNGREN, G. K. & ACRIVOS, A. 1975 Stokes flow past a particle of arbitrary shape; a numerical method of solution. *J. Fluid Mech.* **69**, 377–403 (corrigendum **69**, 813).